

Critical domain wall behavior in chiral magnetic nanowires induced by spin polarized currents

from

Nils Sommer

Master Thesis in Physics
submitted to the Department of Physics, Mathematics and Computer Science
(FB 08)
of Johannes Gutenberg-Universität Mainz
on 2nd of September 2019

last correction on 23rd of September 2019

1st Review: Dr. Karin Everschor-Sitte
2nd Review: Prof. Dr. Friederike Schmid

Ich versichere, dass ich die Arbeit selbstständig verfasst und keine anderen als die angegebenen Quellen und Hilfsmittel benutzt sowie Zitate kenntlich gemacht habe.

Mainz, den 23. September 2019

Nils Sommer
TWIST
Institut für Physik
Staudingerweg 7
Johannes Gutenberg-Universität D-55099 Mainz
nsommer@students.uni-mainz.de

Abstract

The controllable creation and manipulation of magnetic domain walls by electrical currents is an innovative process for the development of a new generation of magnetic memory devices. A recent paper presented a proof of concept of a method for controllable creation of domain walls in a ferromagnetic nanowire. An applied electrical current above a critical threshold in a nanowire with a fixed magnetization at the edge injects domain walls periodically. It was considered for the ferromagnetic wire a minimal model with only exchange interaction and uniaxial anisotropy along the wire. No twisting terms, such as Dzyaloshinskii-Moriya interaction (DMI) and dipole-dipole interaction were considered. It was predicted that these contributions could significantly reduce the required electrical current.

In this thesis we investigate the influence of additional Dzyaloshinskii-Moriya interaction on the creation and behavior of magnetic domain walls. The inversion symmetry broken by the DMI causes the existence of two critical current densities depending on the type of domain wall. Further, we show that the critical current density has a linear dependence on the DMI strength. We analyze the interaction between two domain walls and show that DMI facilitates the annihilation of both domain walls with each other.

We also investigate the domain wall creation by spin orbit torques and show that the critical current density depends linearly on the anisotropy strength and decreases quadratically with the DMI strength.

In addition, we perform micromagnetic simulations to support our theoretical calculations.

We show that the additional twisting term DMI as well as spin orbit torques can reduce the critical current threshold. It facilitates the creation of domain walls with lower current densities and thus reduces the heating of possible devices by the electric current.

Kurzzusammenfassung

Das kontrollierte Erzeugen und Manipulieren magnetischer Domänenwände durch elektrische Ströme ist ein innovatives Verfahren, welches insbesondere Anwendung bei der Entwicklung neuer magnetischer Speichersysteme findet. In einer kürzlich veröffentlichten Publikation wurde ein neues Verfahren zur kontrollierten Erzeugung von Domänenwänden in einem ferromagnetischen Nanodraht vorgestellt. Die erste Magnetisierung des Drahtes wurde senkrecht zum Draht fixiert. Durch einen angelegten elektrischen Strom können an der fixierten Magnetisierung Domänenwände erzeugt werden, sofern die Stromstärke über einem kritischen Wert liegt.

Für den ferromagnetischen Draht wurde ein simples Modell angenommen, welches nur Austauschwechselwirkung und uniaxiale Anisotropie entlang des Drahtes beinhaltet. Terme, die eine verdrehende Wirkung auf die magnetische Textur haben, wie zum Beispiel Dzyaloshinskii-Moriya-Wechselwirkung (DMI) oder Dipol-Dipol-Wechselwirkung, wurden nicht berücksichtigt. Es wurde jedoch vermutet, dass diese Beiträge die erforderliche elektrische Stromstärke deutlich reduzieren können.

In dieser Masterarbeit untersuchen wir den Einfluss zusätzlicher Dzyaloshinskii-Moriya-Wechselwirkung auf die Erzeugung und das Verhalten von magnetischen Domänenwänden im Nanodraht. Unsere Ergebnisse zeigen, dass die durch die DMI gebrochene Inversionssymmetrie dazu führt, dass zwei kritische Stromdichten vorhanden sind, welche sich je einem der beiden Domänenwandarten zuordnen lassen. Darüber hinaus zeigen wir, dass die kritische Stromstärke, welche für die Erzeugung von Domänenwänden notwendig ist, eine lineare Abhängigkeit von der DMI-Stärke aufweist. Weiter analysieren wir das Verhalten der Domänenwände nach ihrer Erzeugung und untersuchen dabei insbesondere die Wechselwirkung zwischen zwei Domänenwänden. Unsere Ergebnisse zeigen, dass DMI die Vernichtung beider Domänenwände untereinander erleichtert.

Eine weitere Methode, welche wir in dieser Arbeit untersuchen, ist die Erzeugung von Domänenwänden mithilfe von Spin Orbit Torques. Wir zeigen, dass die kritische Stromstärke linear von der Stärke der Anisotropie abhängt und quadratisch mit der DMI-Stärke abnimmt.

Ergänzend zu unseren Rechnungen führen wir mikromagnetische Simulationen durch, um unsere theoretischen Vorhersagen zu unterstützen.

Unsere Ergebnisse zeigen, dass die zusätzliche DMI sowie Spin Orbit Torques den kritischen Stromwert reduzieren können. Beide Verfahren erleichtern die Erzeugung von Domänenwänden durch geringere notwendige Stromdichten und könnten so die Erwärmung möglicher Geräte in späteren Anwendungen reduzieren.

Content

1. Introduction	1
2. Micromagnetic interactions and dynamics	3
2.1. Micromagnetic model of a ferromagnet	3
2.2. Dzyaloshinskii-Moriya interaction	4
2.3. Magnetic domain walls	4
2.4. Dynamics of magnetization	6
2.4.1. Landau-Lifshitz-Gilbert equation	6
2.4.2. Spin torques	7
2.5. Dynamics of domain walls	8
2.6. Set-up	10
3. Domain wall creation without DMI by STT	12
4. Domain wall creation with DMI by STT	14
4.1. Ferromagnetic instability	14
4.2. Critical current with bulk DMI	16
4.3. Different shedding frequency	18
4.4. Domain wall velocity and annihilation	19
4.5. Simulation	21
4.5.1. Determination of critical current by squared frequency	22
4.5.2. Determination of critical current by nested intervals	24
4.5.3. Domain wall velocity and interaction	26
5. Domain wall creation without DMI by SOT	30
5.1. Critical current without DMI	30
5.2. Simulation	32
6. Domain wall creation with DMI by SOT	35
6.1. Critical current with DMI	35
6.2. Simulation	37
7. Conclusion and outlook	38
A. Appendix	40
A.1. Nomenclature	40
A.2. Additional figures	40
A.3. Numeric Simulation Codes	45

Content

B. Literature	56
C. Acknowledgment	59

1. Introduction

A central topic in spintronics is the manipulation of magnetic textures. A special interest is on the creation and manipulation of domain walls by electric currents [1, 2, 3, 4, 5, 6, 7] to create new types of magnetic memory devices like racetrack memories [8, 9, 10].

In recent works, a new method for the controllable and periodic creation of magnetic textures was discovered [11, 12, 13, 14]. While most of them concentrate on two dimensional textures, i.e. skyrmions, the mechanism is possible for one-dimensional magnetic systems, i.e. domain walls. In reference [11] the authors demonstrate that domain walls can be periodically injected into magnetic nanowires just by the interplay of an electric current and a local inhomogeneity. The authors consider the following set-up, especially for the analytic treatment. A model of a one dimensional wire containing exchange interaction and anisotropy along the wire. The magnetization at the beginning of the wire is fixed along a perpendicular direction, and the magnetization at infinity orients along the easy axis. The authors showed that domain walls are injected into the nanowire if the current density is above a certain critical value and below the ferromagnetic instability. Furthermore, the period by which the domain walls are injected can be controlled by the current strength.

In this thesis we expand the predictions to a system with additional Dzyaloshinskii-Moriya interaction (DMI). We analyze the effect of DMI on the critical current density and on the behavior of the domain walls after their creation. DMI breaks the symmetry of the two possible domain walls which can occur in the wire. While DMI decreases the velocity and the critical current density for one type of domain wall, it increases these values for the other domain wall type. Further, DMI ease that two domain walls annihilate with each other.

We also investigate the domain wall creation by spin orbit torques. We analyze the process in a wire with and without DMI and show that the critical current density has a linear dependence on the anisotropy strength and decreases quadratically with the DMI strength.

In addition to our analytic calculations we perform micromagnetic simulations and compare the numeric results to our theoretical predictions.

This thesis is divided into five parts. In the first two parts we give a short introduction on micromagnetism and domain walls, and review the main results from reference [11].

1. Introduction

The third part is about the domain wall creation and their behavior in a nano wire with additional Dzyaloshinskii-Moriya interaction. The last two parts are about the domain wall creation by spin orbit torques, with and without the presence of DMI.

2. Micromagnetic interactions and dynamics

2.1. Micromagnetic model of a ferromagnet

In the micromagnetic model of ferromagnetism the state of a magnetic material is described by the vector field of the magnetizations \mathbf{M} [15, 16]. In the ferromagnetic state the magnetization is locally saturated to its saturation magnetization M_s . In this thesis we use the normalized magnetization

$$\mathbf{m} = \frac{\mathbf{M}}{M_s}. \quad (2.1)$$

For the description of a ferromagnet we use two major interactions for the magnetizations. An expansion of the Heisenberg model of the neighboring spin-spin interaction yields to an exchange interaction between neighboring magnetizations. The Hamiltonian of this exchange interaction is [17]

$$\mathcal{H}_{\text{ex}} = -\frac{J}{2} \sum_{i,j} \mathbf{m}_i \cdot \mathbf{m}_j \quad (2.2)$$

where J is the exchange constant and $\mathbf{m}_i, \mathbf{m}_j$ are nearest neighbor magnetizations. The energy is minimized if \mathbf{m}_i and \mathbf{m}_j are parallel ($J > 0$) or antiparallel ($J < 0$). For the case where J is negative the order of the magnetization is alternating and the material gains antiferromagnetic properties. For a positive J all magnetizations aligns parallel and the material is ferromagnetic [18].

Several material conditions, like shape of the ferromagnet, interactions of the magnetizations with the crystal lattice or external magnetic fields, lead to a preferred direction for the magnetization orientation. This effect is called anisotropy. The preferred magnetization direction is the easy axis and it costs energy to deflect magnetization out of this direction. In a system there can be several easy axes, i.e. systems with cubic anisotropy have an easy axis in every three directions of space. In this thesis we focus on a system with only one easy axis. The energy of this interaction reads as [17]

$$\mathcal{H}_{\text{ani}} = -\lambda \sum_i (\mathbf{m}_i \cdot \mathbf{n})^2 \quad (2.3)$$

where $\lambda > 0$ is the anisotropy constant and \mathbf{n} the unit vector of the easy axis.

2. Micromagnetic interactions and dynamics

The energy F of this system is given by the sum of all interactions

$$F = H_{\text{ex}} + H_{\text{ani}} + H_{\text{other}} . \quad (2.4)$$

where H_{other} represents all other possible interactions, i.e. dipole-dipole interaction, interaction with external magnetic fields or Dzyaloshinskii-Moriya interaction.

2.2. Dzyaloshinskii-Moriya interaction

In materials with broken inversion symmetry an additional exchange interaction occurs known as Dzyaloshinskii-Moriya interaction (DMI)[19, 20, 21]. The Hamiltonian of this interaction is

$$\mathcal{H}_{\text{DMI}} = -\mathbf{D} \cdot \sum_{i,j} \mathbf{m}_i \times \mathbf{m}_j . \quad (2.5)$$

This Hamiltonian is minimized if the two nearest neighbor magnetizations \mathbf{m}_i and \mathbf{m}_j are perpendicular to each other, and the cross product of both is parallel to the DMI vector \mathbf{D} . DMI induces a rotation of the magnetization and the DMI vector defines the rotation axis.

The origin of the broken inversion symmetry can be either a lattice structure with no inversion symmetry or an interface between two materials with different lattice structures, so that the lattice is not inversion symmetric at the interface between the materials. The first type is known as bulk induced or Bloch type DMI the other type as surface induced or Néel DMI. Especially, for surface induced DMI the DMI vector is always in the plane of the interface.

2.3. Magnetic domain walls

We now consider a ferromagnetic material with exchange interaction ($J > 0$) and uniaxial anisotropy (only one easy axis). Obviously, the ground state of the system is a set-up where all magnetizations point in the same direction and along the easy axis. The magnetizations can point either in positive or negative direction of the easy axis, so that there are two possible ground states. Especially, there are metastable states where both types of ground states exist. The areas where the magnetizations points parallel or antiparallel to the easy axis are magnetic domains and between two different domains there is a magnetic domain wall. The domain wall characterize as part of the ferromagnet where the magnetization direction changes smoothly from the orientation of one domain to the orientation of the other domain. The typical width of a domain wall is given by the square root of the ratio of exchange and anisotropy constants [22, 18]

2. Micromagnetic interactions and dynamics

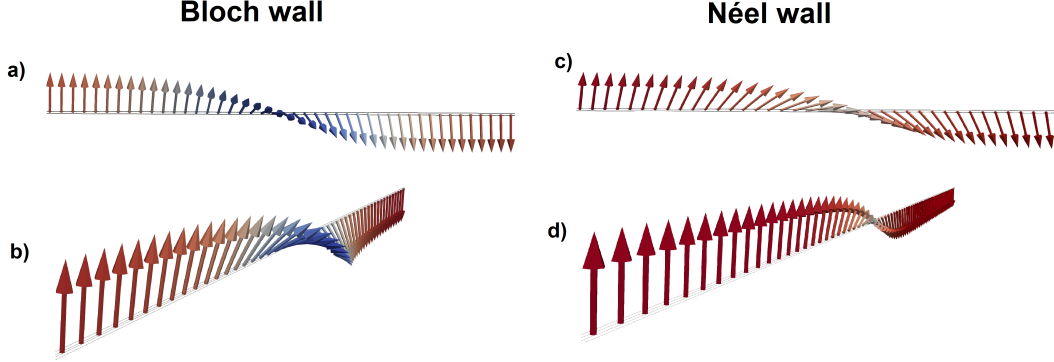


figure 2.1.: On the left side is a Bloch domain wall. a) shows the side view on a Bloch wall b) is a tilted view. The magnetization changes its direction perpendicular to the domain wall direction. On the right side is a Néel type domain wall where c) shows the side view and d) the tilted view. The magnetization changes in the same direction as the domain wall expands. The red areas are the both domains. The blue color shows the y component of the magnetization.

$$\Delta = \sqrt{\frac{J}{2\lambda}}. \quad (2.6)$$

For a set-up where the easy axis is perpendicular to the direction of domain wall, the magnetization direction can change its direction either in the same direction like the direction of the domain wall or perpendicular to it. The first case is a Néel type domain wall the second a Bloch type domain wall. Both types of domain walls are shown in figure 2.1.

If the easy axis is parallel to the direction the domain wall there are also two different types of domain walls. If the magnetization directions of both domains point to each other there is a head to head domain wall between them. If the magnetizations of both domains are pointing away from each other there is a tail to tail domain wall. Both types are shown in figure 2.2.

An effective description of a domain wall is to parameterize it by its position X_0 , where the position X_0 represents the middle of the domain wall. For the head to head and tail to tail domain walls we can add an angle ϕ_0 which represents the angle of the domain wall to a free chosen axis which is perpendicular to the easy axis. The parametrization are shown in figure 2.2 for a tail to tail domain wall [3, 7, 17, 23, 24].

2. Micromagnetic interactions and dynamics

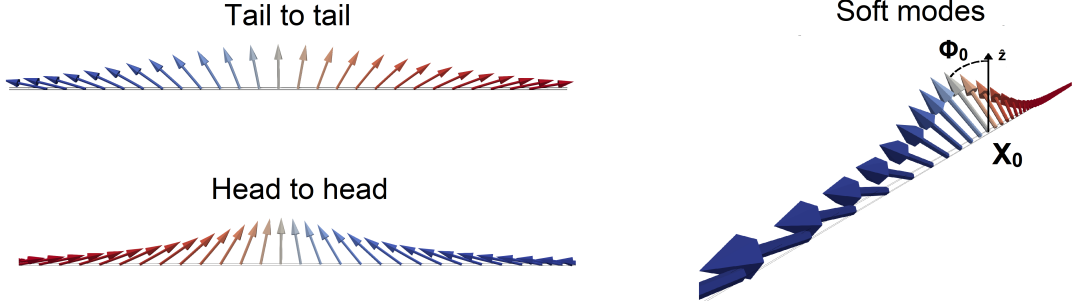


figure 2.2.: A tail to tail and a head to head domain wall in a ferromagnetic material with uniaxial anisotropy. In this set-up a tail to tail domain wall originates if the the magnetization direction changes from a left oriented domain to a right oriented domain. If the magnetization direction changes from a right oriented domain to left oriented domain there is a head to head domain wall. On the right side is a parametrization to describe a domain wall. The position X_0 of the domain wall is defined by the coordinate of the middle of the domain wall. For a head to head or a tail to tail domain wall the orientation of the middle of the domain wall can be described by its relative angle ϕ_0 to the \hat{z} axis.

2.4. Dynamics of magnetization

2.4.1. Landau-Lifshitz-Gilbert equation

The dynamics of the magnetization is described by the Landau-Lifshitz-Gilbert (LLG) equation [25, 26]

$$\dot{\mathbf{m}} = -\gamma \mathbf{m} \times \mathbf{H}_{\text{eff}} + \alpha \mathbf{m} \times \dot{\mathbf{m}} + \boldsymbol{\tau} \quad (2.7)$$

where γ is the gyromagnetic ratio, \mathbf{H}_{eff} an effective magnetic field, α the Gilbert damping and $\boldsymbol{\tau}$ a torque acting on the magnetization \mathbf{m} .

The first part of the equation describes the precession of the magnetization around the effective magnetic field \mathbf{H}_{eff} . The effective magnetic field in a ferromagnet is given by the internal field and external magnetic fields. The internal magnetic field is a field generated by the magnetization and especially describes the interaction between them

$$\mathbf{H}_{\text{eff}} = \mathbf{H}_{\text{internal}} + \mathbf{H}_{\text{external}} = -M_s^{-1} \frac{\delta F[\mathbf{m}]}{\delta \mathbf{m}} + \mathbf{H}_{\text{external}}. \quad (2.8)$$

The second part of the LLG describes the damping of the precession around \mathbf{H}_{eff} . The magnetization aligns parallel to the effective magnetic field after a certain time and α is the Gilbert damping constant.

The third part of the LLG describes external torques generated by spin currents, for

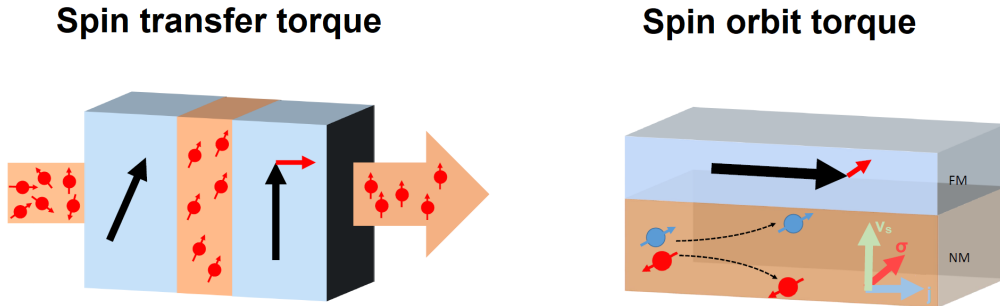


figure 2.3.: On the left is a set-up for a spin transfer torque device. An unpolarized current is injected into the device. A layer with a fixed magnetization direction polarizes the current so the electron spins align parallel to its magnetization. A non magnetic layer separates the magnetic layer from another one. The magnetizations of these layers are not parallel to each other so the spin polarized current acts a torque on the magnetization in the second layer. On the right is a set-up for a spin orbit torque device. There is a non magnetic layer with a magnetic layer on the top. The non magnetic layer has large spin orbit coupling and polarize an electric current by the spin Hall effect. The spin current is injected perpendicular into the magnetic layer. j is the electric current, v_s the spin current velocity and σ the spin current polarization.

example.

2.4.2. Spin torques

Every electron has in addition to its charge another quantity called the electron spin. This spin has an orientation and can be polarized in a certain direction. An electric current can be spin polarized so that all spins of the conduction electrons are oriented in the same direction.

In non-magnetic conductors the spins of the conduction electrons are randomly oriented. However, in ferromagnetic materials with a fixed magnetization direction the spins are forced to align parallel to local magnetization direction and the electric current becomes spin polarized. This process is shown in figure 2.3 a) in the left magnetic layer. Another possibility to create a spin polarized current is using the spin orbit interaction in materials with large spin orbit coupling. The spin hall effect [27, 28, 29] or the Rashba effect [30, 31] separate electrons with opposite spin polarization. This induces a spin polarized current at one surface of the material and on the opposite surface a current with opposite polarization direction.

2. Micromagnetic interactions and dynamics

If a spin polarized current is injected to a magnetic material with a different magnetization direction than the polarization of the spin current, the spins of the electrons align again parallel to the local magnetization direction. The electron spin has properties of an angular momentum and due to conservation of angular momentum the electrons act a torque on the magnetizations in the material. If the direction of the magnetizations is not fixed by some reasons the spin polarized current will change the magnetization direction to the direction of the spin current polarization. The torque an spin polarized current acts on a magnetization is given by

$$\boldsymbol{\tau} = \tau_{FL} \mathbf{m} \times \boldsymbol{\sigma} + \tau_{DL} \mathbf{m} \times (\mathbf{m} \times \boldsymbol{\sigma}) . \quad (2.9)$$

where τ_{FL} is the prefactor of the field like term, τ_{DL} the factor of the damping like term and $\boldsymbol{\sigma}$ the polarization direction of the spin current[31, 32, 33, 34, 35].

There are two different spin torques. The spin transfer torque (STT)[32, 33, 36] and spin orbit torque (SOT) [37, 38, 39, 40]. For the spin transfer torque the electric current is spin polarized by passing a fixed magnetic layer before entering the other magnetic layer with changeable magnetization direction. The set-up is a spin valve which is shown in figure 2.3 a). For a continous spin valve where the magnetization direction changes smoothly its direction the equation for the spin transfer torque can be simplified. The spin transfer torque reads then

$$\boldsymbol{\tau}_{STT} = -(\mathbf{v}_s \cdot \boldsymbol{\partial}) \cdot \mathbf{m} + \beta \mathbf{m} \times (\mathbf{v}_s \cdot \boldsymbol{\partial}) \cdot \mathbf{m} \quad (2.10)$$

where β is damping constant of the damping like torque and \mathbf{v}_s is the spin velocity which represents the spin polarized current. The relation between spin velocity and electric current is given by $\mathbf{j} = \frac{eM_s}{P\mu_B} \mathbf{v}_s$ where e is the electron charge, P the spin polarization and μ_B the Bohr magneton [3, 11].

A possible set-up for a spin orbit torque device is shown in figure 2.3 b). The current is spin polarized by the spin Hall effect in the lower and non magnetic layer and it is injected perpendicular into magnetic layer on the top. The difference to the spin transfer torque is that the spin polarization does not depend on the local magnetization direction of the magnetic layer. Especially, in our case the spin polarization is given by

$$\boldsymbol{\sigma} = \mathbf{j} \times \hat{\mathbf{z}} \quad (2.11)$$

where \mathbf{j} is the electric current and $\hat{\mathbf{z}}$ the normal of the surface between the non magnetic and magnetic films.

2.5. Dynamics of domain walls

The two spin torques (STT, SOT) can move domain walls in a ferromagnetic material. For the moment we are focusing on the movement due to spin transfer torque.

2. Micromagnetic interactions and dynamics

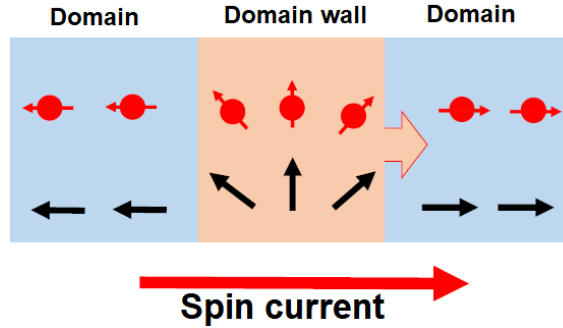


figure 2.4.: The movement of a domain wall by a spin polarized current. The electron current is flowing from left to right. The spin of the electrons align parallel to the local magnetization direction. At the domain wall the direction of the electron spin changes its direction. Because of conservation of angular momentum the direction of the magnetizations of material also change their directions so the domain wall moves in the same direction like the electron current flows.

As it is described in the section 2.4.2 spin polarized currents act a torque on the magnetizations if their orientation is not parallel to the spin polarization direction.

To understand the process of domain wall movement we change the perspective to the perspective of an electron. Imagine a set-up of a one dimensional ferromagnet with two domains where the magnetizations of the first domain are pointing to the left and in the second domain they are pointing in right direction. Between these two domains there is a domain wall where the magnetizations change their orientation smoothly from left to right. (see figure 2.4)

A conduction electron passes the first domain, then the domain wall and finally the second domain. The spin of the electron aligns always parallel to the local magnetization direction. When the electron passes the domain wall it spin changes its direction from left to right. Due to the conservation of angular momentum, the orientation of each magnetization in the domain wall has to change slightly to the left, so that the domain wall moves slightly to the right. Each passing conduction electron moves the domain wall a bit more, so that an electric spin polarized current moves the domain wall in the same direction as the current flows. (see figure 2.4)

The speed of a domain wall in a ferromagnetic material with exchange interaction,

2. Micromagnetic interactions and dynamics



figure 2.5.: Different ground states for a one dimensional nanowire with exchange interaction, anisotropy and DMI. In all wires the first magnetization is fixed in \hat{z} direction. The blue and red colors show the y component of the magnetization. Blue coloration is a positive y component red means negative component. a) shows the wire without DMI. The magnetizations change their direction slightly from the fixed direction to the direction of the easy axis. So a 90 degree domain wall is formed after the fixed magnetization. b) shows the nanowire with small DMI strength below the critical strength $D^2 < D_c^2 = 2J\lambda$. The DMI yields to a twist of the magnetization in \hat{y} direction behind the fixed one. c) shows the nanowire where the DMI strength is larger than the critical value. Here the magnetization form a spiral around the wire with a pitch of $2\pi\frac{J}{D}$. For b) and c) the direction of the twist and winding depends on the sign of the DMI strength D .

anisotropy and DMI is given by [22]

$$\dot{X}_0 = \frac{1 + \alpha\beta + (\alpha - \beta)\Gamma\Delta_0}{1 + \alpha^2}v_s \quad (2.12)$$

where $\Gamma = D/J$ is the ratio of DMI strength and exchange constant, and $\Delta_0^{-2} = \Delta^{-2} + \Gamma^2$ with Δ as the domain wall width without DMI (see eq. 2.6).

2.6. Set-up

In this thesis we consider a set-up of one dimensional semi-infinite ferromagnetic nanowire oriented along \hat{x} direction with exchange interaction and uniaxial anisotropy along the wire. The first magnetization of the wire is fixed in \hat{z} direction. In section 2.1 and 2.2 we describe the energy for a discrete model. For a continuous model with bulk induced DMI the energy reads as

$$F[\mathbf{m}] = \int_0^\infty dx \left[\frac{J}{2} (\partial_x \mathbf{m})^2 + \lambda (1 - m_x^2) + D \mathbf{m} \cdot (\nabla \times \mathbf{m}) \right] \quad (2.13)$$

where D is the DMI strength [11, 22].

For a system without DMI ($D = 0$) there is only exchange and anisotropy. The

2. Micromagnetic interactions and dynamics

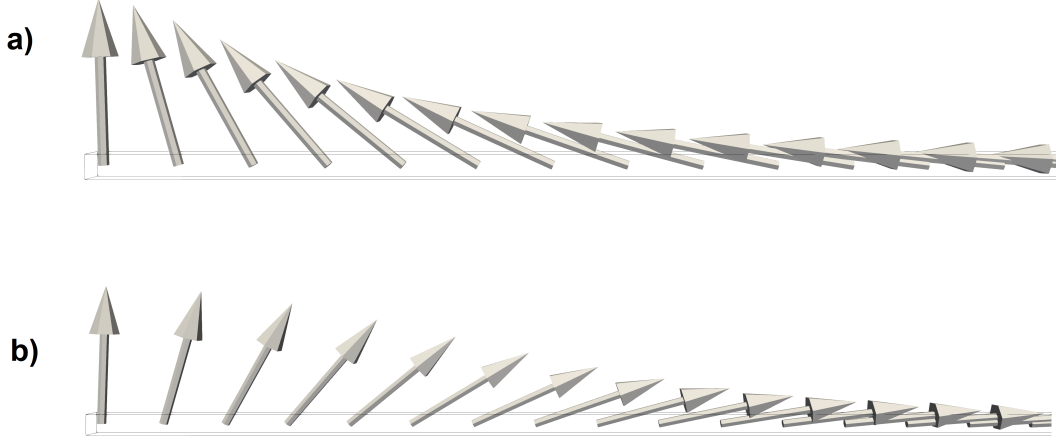


figure 2.6.: There are two possible ground states for the system. The first magnetization is fixed the other magnetization can either align in parallel to the easy axis or anti parallel to it. The energy for both states is the same.

anisotropy prefers that the magnetizations align parallel to the easy axis. Due to exchange interaction the magnetization change smoothly their direction from the fixed direction \hat{z} to the \hat{x} direction so a 90 degree domain wall arises at the beginning of the wire (see figure 2.5 (a)).

For a set-up with DMI there is an interplay between exchange interaction and DMI. The DMI prefers a perpendicular angle between nearest neighbor magnetizations but the exchange interaction tries to align them parallel. This leads to a spiral structure with a pitch $2\pi\frac{J}{D}$. Furthermore there is a critical value of the DMI strength $D_c^2 = 2\lambda J$ which separates two phases of the set-up (figure 2.5(b) and (c))[22, 41].

For DMI strength above this critical value the system is in the helical phase where the magnetizations form a spiral around the wire (figure 2.5 (c)). Below the critical value the system looks quite similar to the set-up without DMI. The magnetization direction changes smoothly from \hat{z} direction to \hat{x} direction. But due to DMI there is a small twist of the magnetization out of the x-z plane in the gradient after the fixed magnetization (figure 2.5(b)).

Furthermore, the ground state of the system below the critical DMI strength is degenerate. The magnetization at infinity can either point along the positive \hat{x} direction or in negative \hat{x} direction. Both states are shown in figure 2.6.

3. Domain wall creation without Dzyaloshinskii-Moriya interaction by spin transfer torque

In this chapter we review the results of reference [11]. In this publication the creation of magnetic domain walls by spin transfer torque in nanowires with exchange interactions and anisotropy along the wire is predicted. It is the same set-up like the set-up without DMI which was described in section 2.6. The two ground states are described in the previous section and they are shown in figure 2.6 a) and b). For the analytics the authors focused on the ground state with $m_x = 1$ for $x \rightarrow \infty$ (figure 3.1). The calculation for the other ground state is analog. The free energy of the system is given by

$$F[\mathbf{m}] = \int_0^\infty dx \left[\frac{J}{2} (\partial_x \mathbf{m})^2 + \lambda (1 - m_x^2) \right]. \quad (3.1)$$

Applying a small spin polarized current the magnetizations behind the fixed magnetization are twisted out of the x-z plane (fig. 3.1 (2)), but for a constant current density the system is still stable. As the current strength increase, the twist of the magnetization becomes larger. Above a critical current density $j_c = \frac{e\gamma}{P\mu_B} \sqrt{2\lambda J}$ the system becomes unstable and domain walls are injected periodically into the wire (fig. 3.1 (3)).

The authors showed that the creation of domain walls is periodic with a period of

$$T = \frac{\sqrt{2\pi e^2 J M_s \gamma}}{j_c^2 P^2 \mu_b^2} \sqrt{\frac{j_c}{j - j_c}}. \quad (3.2)$$

After the creation the domain walls are moving through the wire due to spin transfer torque.

The bachelor thesis of Nils Sommer [42], which is based on this reference [11], deals with the influence of the orientation of fixed magnetization. The results show that the critical current density has a minimum if the magnetization is fixed perpendicular to the wire.

3. Domain wall creation without DMI by STT

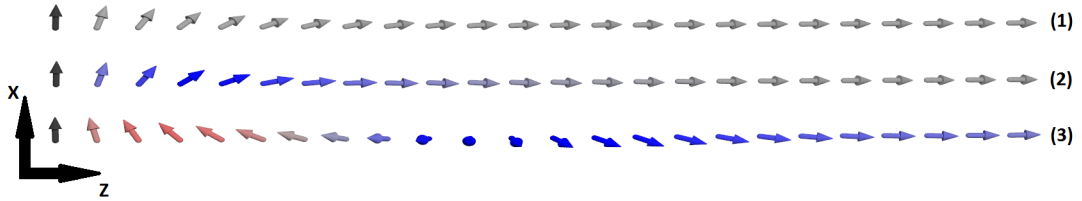


figure 3.1.: Set-up of a ferromagnetic wire. The first magnetization (colored black) is fixed perpendicular to the wire. (1) is the ground state where the magnetizations orient themselves due to exchange interaction and anisotropy. (2) shows the state with an applied current j which is smaller than the critical current value $j < j_c$. The magnetizations after the fixed magnetization are twisted out of the x-z plane. The coloration of the magnetization defines the y-component. Blue is in positive y-direction red in negative. (3) shows the unstable state where the current strength is above its critical value $j > j_c$ and domain walls are created periodically. A domain wall is shown which was created at the beginning and is now moving through the wire. This figure was created in style of the figure 1 from ref. [11].

4. Domain wall creation with Dzyaloshinskii-Moriya interaction by spin transfer torque

In this chapter we investigate the creation of domain walls and their behavior in a ferromagnetic nanowire due to additional Dzyaloshinskii-Moriya interaction. In the first part we calculate the new critical current density and demonstrate the influence of DMI on the created domain walls. In the second part we compare our analytic results to micromagnetic simulations.

In the following chapters we use similar calculations to determine the critical current value. Therefore we show a detailed calculation of the critical current density in this chapter. In the other chapters we only describe the main steps which show the important differences between the calculations.

4.1. Ferromagnetic instability

Besides the critical current for the domain wall creation there is a second critical current value for the ferromagnetic instability. For electric currents above this critical current value the magnetic material loses its ferromagnetic properties [11][43]

To calculate the ferromagnetic instability we use the implicit form of the Landau-Lifshitz-Gilbert equation with spin transfer torque

$$(1 + \alpha^2) \dot{\mathbf{m}} = -\gamma \mathbf{m} \times \mathbf{H}_{\text{eff}} - \alpha \gamma \mathbf{m} \times (\mathbf{m} \times \mathbf{H}_{\text{eff}}) - (1 - \alpha\beta) v_s \partial_x \mathbf{m} + (\beta - \alpha) v_s \mathbf{m} \times \partial_x \mathbf{m}. \quad (4.1)$$

The effective magnetic field reads

$$\mathbf{H}_{\text{eff}} = -M_s^{-1} \frac{\delta F[\mathbf{m}]}{\delta \mathbf{m}} = \frac{1}{M_s} \left(J \partial_x^2 \mathbf{m} + 2\lambda m_x \hat{\mathbf{x}} + 2D ((\partial_x m_z) \hat{\mathbf{y}} - (\partial_x m_y) \hat{\mathbf{z}}) \right). \quad (4.2)$$

The magnetic state $\mathbf{m} = \mathbf{m}_0 + \mathbf{s}$ is the ferromagnetic ground state $\mathbf{m}_0 = \hat{\mathbf{x}}$ plus a small perturbation \mathbf{s} with $s^2 \rightarrow 0$ and $\hat{\mathbf{x}} \perp \mathbf{s}$. For \mathbf{s} we use a spin wave ansatz

$$\mathbf{s} = e^{i(kx - \omega t)} (f \hat{\mathbf{y}} + g \hat{\mathbf{z}}). \quad (4.3)$$

4. Domain wall creation with DMI by STT

If $\text{Im}(\omega) > 0$ the spin wave increases its amplitude in time and the system becomes unstable. Further, if $\text{Im}(k) \neq 0$ the amplitude of the spin wave increases in space so we have two conditions for the stability of our system.

Using this perturbation ansatz, the implicit LLG (4.1) gives us

$$0 = \begin{bmatrix} a & b \\ -b & a \end{bmatrix} \mathbf{s} \quad (4.4)$$

with

$$a = \frac{\alpha\gamma}{M_s} (2\lambda + k^2 J) + i \left[\omega (1 + \alpha^2) - \frac{2k\gamma}{M_s} D - kv_s (1 + \alpha\beta) \right]$$

$$b = -\frac{\gamma}{M_s} (2\lambda + k^2 J) + i \left[-\frac{2k\gamma}{M_s} D + kv_s (\beta - \alpha) \right].$$

To solve the equation (4.4) the determinant of the matrix has to be equal to zero $a^2 + b^2 = 0$. This equation gives us two solutions for ω

$$\omega_1 = \frac{[kv_s M_s + kv_s M_s \alpha\beta + 2Dk\gamma + Jk^2\gamma + 2\gamma\lambda] + i [J\alpha\gamma k^2 + (v_s M_s \alpha - v_s M_s \beta + 2D\gamma) k + 2\alpha\gamma\lambda]}{M_s (1 + \alpha^2)}$$

$$\omega_2 = \frac{[kv_s M_s + kv_s M_s \alpha\beta + 2Dk\gamma - Jk^2\gamma - 2\gamma\lambda] + i [J\alpha\gamma k^2 - (v_s M_s \alpha - v_s M_s \beta + 2D\gamma) k + 2\alpha\gamma\lambda]}{M_s (1 + \alpha^2)}.$$

The condition $\text{Im}(\omega) < 0$ gives conditions for the wavenumbers k_1 and k_2

$$-c - id < k_1 < -c + id$$

$$c - id < k_2 < c + id$$

with

$$c = \frac{v_s M_s (\alpha - \beta) + 2D\gamma}{2J\alpha\gamma}$$

$$d = \sqrt{\frac{(v_s M_s (\alpha - \beta) + 2D\gamma)^2 - 8J\lambda\alpha^2\gamma^2}{4J^2\alpha^2\gamma^2}}.$$

The second condition that $\text{Im}(k) = 0$ forces that the argument of the square root has to be equal to zero ($d = 0$). With this we get a condition for the spin current velocity v_s

$$\frac{\gamma (2\alpha\sqrt{2J\lambda} - D)}{M_s (\alpha - \beta)} > v_s > \frac{\gamma (-2\alpha\sqrt{2J\lambda} - D)}{M_s (\alpha - \beta)}. \quad (4.5)$$

Especially, for the case without DMI ($D = 0$) and ($\beta = 0$) the ferromagnetic instability is twice the critical current $v_s < 2\frac{\gamma}{M_s}\sqrt{2\lambda J}$ like it was predicted in [11].

4. Domain wall creation with DMI by STT

For the other ground state $\mathbf{m} = -\hat{\mathbf{x}}$ the sign in front of the DMI strength D changes. That means that DMI increases the critical current density of the ferromagnetic instability for one ground state while it decreases this value for the opposite ground state. For a reverse current direction the previously stabilized ground state is now the state with the lower ferromagnetic stability. In a set-up with at least one domain wall both ground states are present so the lower current defines the limit for the ferromagnetic stability.

4.2. Critical current with bulk DMI

In this section we show that the critical current for the domain wall creation in a ferromagnetic wire with DMI is

$$j_c = \frac{e\gamma}{P\mu_B} \left(\pm D + \sqrt{2J\lambda} \right) \quad (4.6)$$

where e is the electron charge, γ the gyromagnetic ratio, P the spin current polarization, μ_B the Bohr-magneton and D the DMI strength. The critical current density depends linear on the DMI strength and for $D = 0$ the critical current density for the system without DMI is recovered [11].

For the calculation we use the conservation of linear momentum and angular momentum. These conservation laws lead to constant derivatives of the magnetization in space at the beginning of the wire.

For our calculations we consider a stable system $\dot{\mathbf{m}} = 0$ and by this we define a condition for the value of spin velocity v_s . Since there are no dynamics, the damping parts of the LLG do not contribute. The LLG without damping terms reads

$$\dot{\mathbf{m}} = -\gamma \mathbf{m} \times \mathbf{H}_{\text{eff}} - (\mathbf{v}_s \cdot \boldsymbol{\partial}) \cdot \mathbf{m} = 0. \quad (4.7)$$

The effective magnetic field is (equation (2.13))

$$\mathbf{H}_{\text{eff}} = \frac{1}{M_s} \left(J\partial_x^2 \mathbf{m} + 2\lambda m_x \hat{\mathbf{x}} + 2D (\partial_x m_z \hat{\mathbf{y}} - \partial_x m_y \hat{\mathbf{z}}) \right). \quad (4.8)$$

The wire is one-dimensional, so we only have to consider the x-component of the LLG. Using the expression for the effective magnetic field, the LLG for the $\hat{\mathbf{x}}$ -component is

$$\dot{m}_x = -\frac{\gamma}{M_s} \left(J\hat{\mathbf{x}} \cdot (\mathbf{m} \times \partial_x^2 \mathbf{m}) - 2D (m_z \partial_x m_z - m_y \partial_x m_y) \right) - v_s \partial_x m_x \quad (4.9)$$

$$= \partial_x \left(-\frac{\gamma}{M_s} \left(J\hat{\mathbf{x}} \cdot (\mathbf{m} \times \partial_x \mathbf{m}) - D m_x^2 \right) - v_s m_x \right) = 0. \quad (4.10)$$

4. Domain wall creation with DMI by STT

This expression indicates that the term inside the brackets is a conserved quantity. The value of this constant can be calculated for $x \rightarrow \infty$ where $m_x = 1$ and $\partial_x \mathbf{m} = 0$. We obtain

$$\frac{\gamma}{M_s} \left(J \hat{\mathbf{x}} \cdot (\mathbf{m} \times \partial_x \mathbf{m}) - D m_x^2 \right) + v_s m_x = v_s - \frac{\gamma}{M_s} D. \quad (4.11)$$

At the beginning of the wire where $\mathbf{m} = \hat{\mathbf{z}}$ equation (4.11) gives us the first constant derivative

$$-\frac{\gamma}{M_s} J \partial_x m_y = v_s - \frac{\gamma}{M_s} D \quad (4.12)$$

$$\partial_x m_y = \frac{D - \frac{v_s M_s}{\gamma}}{J}. \quad (4.13)$$

For the second derivative we have a look on the free energy of the system (equation (2.13)). If we consider the energy as an action of some model and x as the time we obtain the Lagrangian of the model

$$\mathcal{L} = \frac{J}{2} (\partial_x \mathbf{m})^2 + \lambda (1 - m_x^2) + D \mathbf{m} \cdot (\nabla \times \mathbf{m}) \quad (4.14)$$

and the corresponding Hamiltonian

$$\mathcal{H} = \frac{\partial \mathcal{L}}{\partial (\partial_x \mathbf{m})} \partial_x \mathbf{m} - \mathcal{L} = \frac{J}{2} (\partial_x \mathbf{m})^2 - \lambda (1 - m_x^2). \quad (4.15)$$

The fact that the Lagrangian does not depend explicitly on the *time* x implies that the Hamiltonian is conserved. The conservation constant we can calculate again for $x \rightarrow \infty$

$$\frac{J}{2} (\partial_x \mathbf{m})^2 - \lambda (1 - m_x^2) = 0 \quad (4.16)$$

and we get as second constant derivative

$$(\partial_x \mathbf{m})^2 = \frac{2}{J} \lambda (1 - m_x^2). \quad (4.17)$$

For the fixed magnetization at the beginning of the wire where $\mathbf{m} = \hat{\mathbf{z}}$ and $(\partial_x \mathbf{m})^2 = (\partial_x m_x)^2 + (\partial_x m_y)^2$ the two solutions for $(\partial_x \mathbf{m})^2$ and $\partial_x m_y$ (equation 4.13 and 4.17) gives

$$(\partial_x m_x)^2 = \frac{2\lambda}{J} - \left(\frac{D - \frac{v_s M_s}{\gamma}}{J} \right)^2 > 0. \quad (4.18)$$

For stable solution $\partial_x m_x \in \mathbb{R}$ and $(\partial_x m_x)^2 > 0$. Setting the above equation equal to zero we can calculate the critical value for v_s

$$v_s^c = \frac{\gamma}{M_s} \left(D \pm \sqrt{2J\lambda} \right). \quad (4.19)$$

4. Domain wall creation with DMI by STT

Because of $D < D_c = \sqrt{2J\lambda}$ the \pm sign in front of the root determines the current direction. For our calculations we consider positive current directions.

Repeating this calculation for the other ground state $\mathbf{m} = (-1, 0, 0)$ for $x \rightarrow \infty$ we obtain the solution

$$v_s^c = \frac{\gamma}{M_s} \left(-D + \sqrt{2J\lambda} \right). \quad (4.20)$$

The critical current corresponding to the spin velocities is

$$j_c = \frac{eM_s}{P\mu_B} v_s^c = \frac{e\gamma}{P\mu_B} \left(\pm D + \sqrt{2J\lambda} \right). \quad (4.21)$$

There are two solutions for the critical current depending on the type of the ground state (figure 2.6) and it defines the sign in front of the DMI strength D . The type of ground state determines the type of domain wall that will be generated next. So the critical current is directly correlated to the type of the next domain wall. During periodic domain wall creation the type of the ground state switches after every created domain wall. Thus, the critical current density also changes between its two possibilities after every created domain wall.

Furthermore, if the DMI strength going to its critical value $D_c^2 = 2J\lambda$ the critical current density reaches the ferromagnetic instability of one ground state.

4.3. Different shedding frequency

As described in chapter 3 the frequency with that domain walls are created is proportional to the square root of the difference between current and critical current [11]

$$f = \frac{j_c^2 P^2 \mu_B^2}{\sqrt{2\pi} e^2 J M_s \gamma} \sqrt{\frac{j - j_c}{j_c}}. \quad (4.22)$$

For a ferromagnetic wire with DMI there are two different critical current densities depending on the type of domain wall which has to be created next (see equation (4.21)). This means that both domain wall types have their own creation time T_1 and T_2 . Equation (4.22) tells us that the domain wall with the lower critical current has a higher creation frequency and by this a lower creation period than the other type of domain wall. During the periodical creation process the type of domain which is created is alternating. The different creation time for each domain wall type causes that the initial distance between the domain walls is different. More precisely, there are two different distances which are alternating due to the alternating types of domain walls (see. fig 4.1 and fig. 4.2).

4. Domain wall creation with DMI by STT

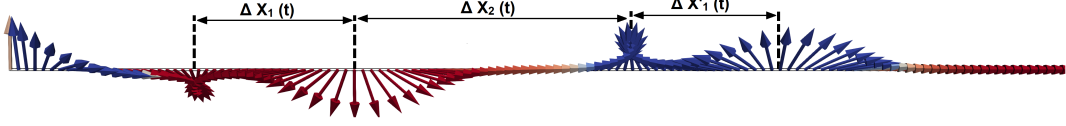


figure 4.1.: Periodic Domain wall creation in ferromagnetic wire with DMI. The color shows the y component of the magnetization (red negative y-component, blue positive y-component). The tail-to-tail domain wall has the higher critical current density and by this a longer creation time. Going from left to right the distance between a head-to-head and a tail-to-tail domain wall ΔX_1 is smaller than the distance between the domain walls in opposite order ΔX_2 . The distances between the domain walls are not constant in time due to their different velocities and the interaction between them.

4.4. Domain wall velocity and annihilation

The velocity of the domain walls (see equation (2.12)) depends on the DMI strength. For small DMI strength we can use a linear approximation

$$\dot{X}_0 = \frac{(1 + \alpha\beta) v_s}{1 + \alpha^2} \pm D \frac{(\alpha - \beta) v_s}{\sqrt{2J\lambda}(1 + \alpha^2)}. \quad (4.23)$$

The domain wall velocity depends also on the type of the domain wall which causes the \pm sign of the DMI strength. The tail to tail domain wall has again the plus sign and the head to head domain wall the minus sign. Interestingly, the domain wall which is created faster is the domain wall with the smaller velocity. These two different speeds yield to the case that one domain wall reaches the other one during their movement in the wire.

Additional to this effect the domain walls interact with each other depending, among other effects, on their distance and the azimuthal angle between them. We approximate the interaction by a long distance approximation in an infinite wire. We assume two rigid domain walls with a separation bigger than the domain wall width Δ . By this only the tails of the domain walls interact with each other.

At the area between the two domain walls the magnetic state is approximately given by

$$\mathbf{m} = \hat{\mathbf{x}} + \mathbf{m}_1 + \mathbf{m}_2 \quad (4.24)$$

where \mathbf{m}_1 and \mathbf{m}_2 describes the tails of the domain walls with $\mathbf{m}_{1,2}^2 \rightarrow 0$ and $\mathbf{m}_{1,2} \perp \hat{\mathbf{x}}$.

The shape of the tails are given by [22]

$$\mathbf{m}_{1,2} = \left(0, \frac{\cos[\Gamma(x - X_{1,2}) + \phi_{1,2}]}{\cosh[(x - X_{1,2})/\Delta_0]}, \frac{\sin[\Gamma(x - X_{1,2}) + \phi_{1,2}]}{\cosh[(x - X_{1,2})/\Delta_0]} \right) \quad (4.25)$$

4. Domain wall creation with DMI by STT

where X_1 and X_2 are the position of the domain walls, ϕ_1 and ϕ_2 their rotation angles measured as angle to the \hat{z} axis, $\Gamma = \frac{D}{J}$ and $\Delta_0^{-2} = \Delta^{-2} + \Gamma^2$.

Using this parametrization of the magnetization the energy reads

$$F = \int dx \left[\frac{J}{2} \left((\partial_x \mathbf{m}_1)^2 + (\partial_x \mathbf{m}_2)^2 \right) + D (\hat{x} \cdot (\nabla \times \mathbf{m}_1 + \nabla \times \mathbf{m}_2)) + J \partial_x \mathbf{m}_1 \cdot \partial_x \mathbf{m}_2 + D (\mathbf{m}_2 \cdot (\nabla \times \mathbf{m}_1) + \mathbf{m}_1 \cdot (\nabla \times \mathbf{m}_2)) \right].$$

For the ordering of the domain wall we define $X_1 < X_2$ and for the large separation $X_1 \ll -\Delta$ and $X_2 \gg \Delta$. By this we can approximate the cosh function (equation (4.25)) by

$$\cosh(x) \rightarrow \frac{e^x}{2} \quad \text{for } x \rightarrow \infty.$$

With this we can do an approximation for the shapes of the tails

$$\mathbf{m}_1 = \left(0, 2 \cos [\Gamma(x - X_1) + \phi_1] e^{-(x-X_1)/\Delta_0}, 2 \sin [\Gamma(x - X_1) + \phi_1] e^{-(x-X_1)/\Delta_0} \right) \quad (4.26)$$

$$\mathbf{m}_2 = \left(0, 2 \cos [\Gamma(x - X_2) + \phi_2] e^{(x-X_2)/\Delta_0}, 2 \sin [\Gamma(x - X_2) + \phi_2] e^{(x-X_2)/\Delta_0} \right). \quad (4.27)$$

Using the above approximation we obtain for the interaction part of the energy

$$F_{interaction} = - \int dx e^{\frac{-|x_1-x_2|}{\Delta_0}} \left[\frac{1}{4J\Delta_0} \left(D^2 \Delta_0^2 - J^2 \right) \cos (\Gamma (x_1 - x_2) + \phi_2 - \phi_1) \right]. \quad (4.28)$$

This equation shows that the interaction increases exponential with decreasing distance between the domain walls. The argument of the cos function defines the sign of the interaction and by this if the interaction is attractive or repulsive. Without DMI ($\Gamma = 0$) the interaction only depends on the relative angle between the two domain walls $\phi = |\phi_2 - \phi_1| < \pi$. If $\phi < \frac{\pi}{2}$ the interaction is attractive, for $\phi > \frac{\pi}{2}$ the interaction is repulsive.

For a system with DMI the interaction also depends on the separation distance of the domain walls. As described in section 2.6 the pitch of the spiral due to DMI is $\frac{2\pi}{\Gamma}$. If the distance between the domain walls is exactly one spiral length $X_2 - X_1 = \frac{2\pi}{\Gamma}$ the energy is minimized for a relative angle $\phi = 0$. For $X_2 - X_1 = \frac{\pi}{\Gamma}$ (half a spiral length) the favored relative angle is $\phi = \pi$. Note, for this case the interaction is attractive but for the case without DMI the interaction is repulsive for a relative angle of $\phi = \pi$

4. Domain wall creation with DMI by STT

However, both domains move in the same direction but rotate in opposite direction around the wire. Thus, the relative angle has bigger effect on the domain wall interaction, especially whether the interaction is attractive or repulsive.

4.5. Simulation

In addition to our analytics we perform micromagnetic simulations with the simulation tool MicroMagnum [44]. MicroMagnum uses finite distance method to perform the time evolution of a magnetic system numerically. It calculates the consecutive configuration of the magnetization with given time steps according to LLG.

Our simulation code is a python script where we define the material parameters (i.e. exchange constant, anisotropy strength, DMI strength, saturation magnetisation) and the set-up. As set-up we use a ferromagnetic wire with 1024 lattice sites. The magnetization are placed along the \hat{x} axis with 3 nm lattice constant. To avoid boundary effects due to DMI [41, 45] we fix the first 100 magnetization in \hat{z} -direction by a strong local magnetic field. The value of the parameters we use in our simulation are listed in the following list.

Parameter	Value
Saturation magnetization M_s	$6 \cdot 10^5 A/m$
Exchange constant J	$2.6 \cdot 10^{-11} J/m$
Anisotropy strength λ	$1 \cdot 10^4 J/m^3$
DMI strength D	$[-15 \cdot 10^{-5}, 15 \cdot 10^{-5}] J/m^2$
Fixing magnetic field strength	$1 \cdot 10^7 A/m$
Spin current polarization P	0.56
Current strength	$\sim 10^{12} A/m^2$

The first part of the simulation is to find the ground state of the system. The initial state is a set of magnetizations where all fixed magnetizations orient along \hat{z} direction and all other magnetizations point in positive or negative \hat{x} direction, depending on which of the two possible ground states has to be the initial state. The simulation finds the set with minimal energy via torque minimization. If the biggest change of a magnetization direction is smaller than 1 *deg/ns* the relaxation process stops and the current state is exported as ground state of the system.

The second part of the simulation is the simulation of the system with an applied current. Our set-up is oriented in positive \hat{x} direction so the domain walls shall move in positive \hat{x} direction. Therefore, we apply a negative current so the electron current is in positive \hat{x} direction. Applying a discrete current pulse above the critical current density is a rapid change in energy and can disrupt the system. To avoid this, we

4. Domain wall creation with DMI by STT

ramp up the current smoothly from zero to a current slightly above the critical current density. For the current ramp up we use a cosine function. The current density at time t is given by

$$\mathbf{j}(t) = j_1 \left(\frac{1.0 - \cos\left(\frac{t}{\tau}\pi\right)}{2}, 0, 0 \right) \quad (4.29)$$

where j_1 is the final current density and τ current ramp up time. After the time τ the current density is equal to j_1 , the current ramp up stops and the current strength is constant

$$\mathbf{j}(t) = j_1 \hat{\mathbf{x}}. \quad (4.30)$$

During the relaxation process, the current ramp up and the simulation with constant current density the ongoing magnetic state is exported after a chosen time step. As default we use a time step of $0.1ns$. Only if a better time resolution is needed we decrease the time step.

In the following section we compare the simulation data with our analytics for the domain wall creation in ferromagnetic wire with DMI by spin transfer torque.

4.5.1. Determination of critical current by squared frequency

In reference [11] the authors determine the critical current by using that the current density is proportional to the squared creation frequency (equation 4.22). In this section we will use the same method to determine the critical current from our simulation.

We simulate the domain wall creation for different DMI strengths in the range of $-15 \cdot 10^{-5} J/m^2$ to $15 \cdot 10^{-5} J/m^2$ with a step size of $5 \cdot 10^{-5} J/m^2$. For each DMI strength we simulate the system for different current densities, larger than the critical current density. Every simulation we perform for four different Gilbert damping α ($\alpha = [0.2, 0.3, 0.4, 0.5]$).

To determine the creation frequency we have a look on the dynamics of the 50th lattice site after the last fixed magnetization. We disassemble the magnetization vector in two components. One component describes the magnetization along the wire M_x the other component the perpendicular part to the wire $m_{\perp} = 1 - m_x^2$. In figure 4.2 (a) the perpendicular component m_{\perp} is plotted versus the time. Every peak represents a passing domain wall. One can see the different creation times T_1 and T_2 due to the different effects of DMI on the two types of domain walls. We assume the maximum of the peak as the time when the domain wall passes the 50th lattice site. For every domain wall pair we calculate the difference between these two times to get all the creation times T_1 and T_2 . The corresponding creation

4. Domain wall creation with DMI by STT

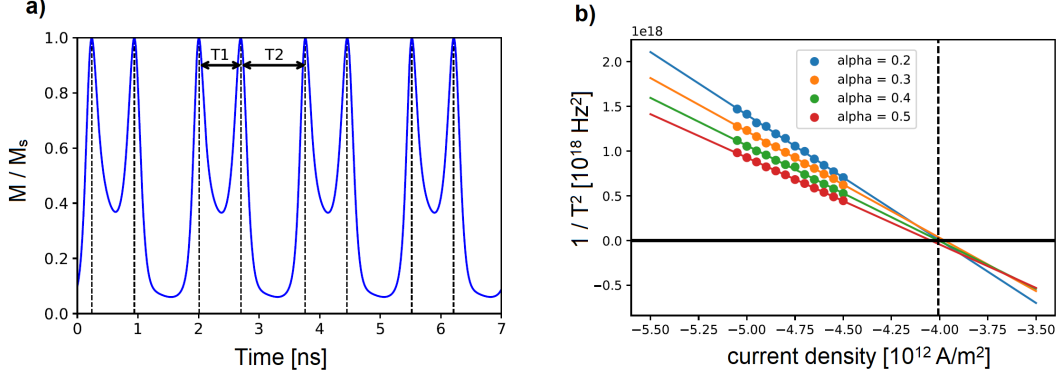


figure 4.2.: We executed simulations for different DMI strengths, current densities j and Gilbert dampings α . For every simulation we analyze the change of magnetization at the 50th lattice site after the fixed magnetization (a). We determine the time difference between two domain walls passes the 150th lattice site. Due to DMI there are two different creation times T_1 and T_2 . We determined these times several times during a simulation and took the average value. We obtain for every DMI strength a set of T_1 and T_2 and the corresponding current density and Gilbert damping. In (b) the creation times T_2 are plotted versus the currents density and all points with the same Gilbert damping α are fitted linear. The x axis section represents the critical current density from the measurements for one Gilbert damping. As critical current we chose the means value out of the four. The analysis for the critical current corresponding to T_1 is analog.

frequency f_1, f_2 we calculate by inverting the mean values of the creation times $f = \frac{1}{T}$.

In the end we obtain for every DMI strength a data set containing pairs of the creation time and the corresponding current strength for both types of domain walls. For one domain wall type and the same value of α the squared creation frequency is proportional to the current strength. We fit the pairs of squared creation time and current strength by a line for every value of α (see figure 4.2 (b)). The current density where $f^2 = 0$ is the critical current density. We calculate the critical current density for every DMI strength and domain wall type as mean value of the critical current densities from all four fits. The graphic A.1 shows the determination process.

The results of the critical current densities for different DMI strengths are shown in figure 4.3. For the set-ups with DMI ($D \neq 0$) there are two different critical currents, one for each type of domain wall. For one type of domain wall the critical current density decreases with increasing DMI strength while the critical current density increases for the other type of domain wall. Further, there is a difference between our theore-

4. Domain wall creation with DMI by STT

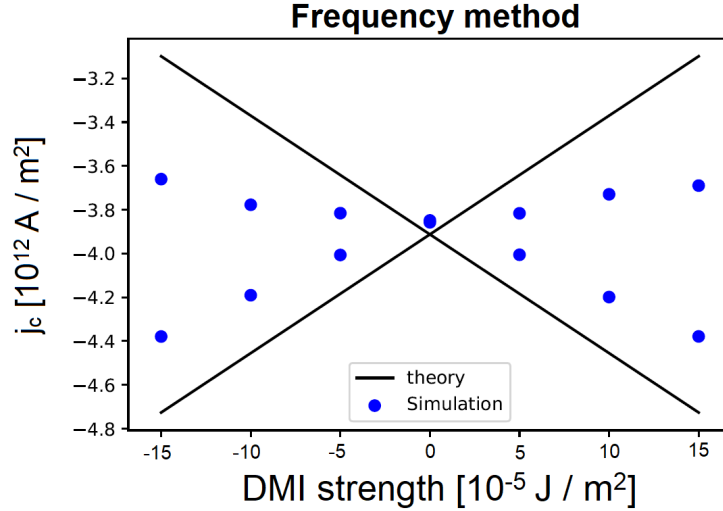


figure 4.3.: Results of the simulation and determination of the critical current with the frequency method. There are two different critical currents for the systems with DMI. The results from the simulation do not fit well with our theory what can be explained due to the interaction of the domain walls with each other.

tical predictions and the simulation result which increases for higher DMI strengths. We suppose that this difference comes from the interaction between the domain walls. By this the measured time at the 50th lattice site after the last fixed magnetization is not the same like the initial time difference during the creation at the last fixed magnetization. Therefore, there are different results for analysis at different lattice sites (see Appendix figure A.4).

4.5.2. Determination of critical current by nested intervals

Another possibility to determine the critical current is to use the method of nested intervals.

To determine if domain walls are created we analyze again the dynamics of a magnetization in a short distance behind the last fixed magnetization. If the sign of the x component of this magnetization changes in time a domain wall passed this magnetization. If there is no domain wall creation the sign of the x component is constant in time. For current density above but very close to critical current density the creation time goes to infinity, so we have a resolution limited by the simulation time. We choose a simulation time of 100ns so we cannot detect domain walls with a creation time of more than 100ns .

4. Domain wall creation with DMI by STT

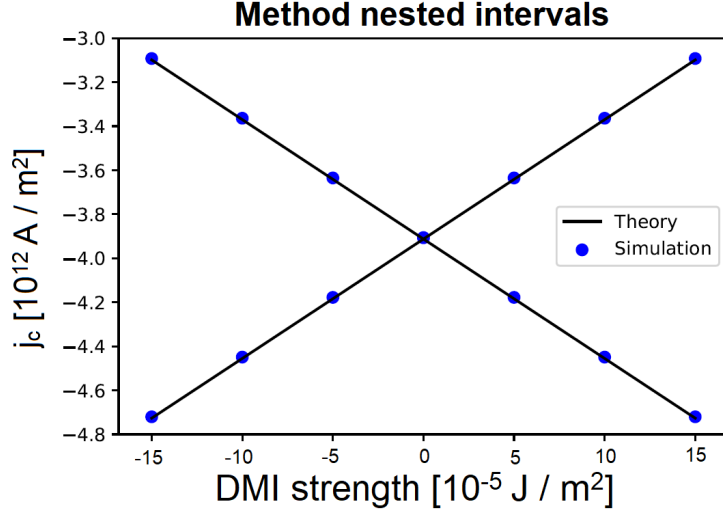


figure 4.4.: Results of the simulation and determination of the critical current density with the nested interval method. There are two different critical currents for the systems with DMI. The intervals of the critical current density have a range of $\sim 4\%$ and are too small to be seen in this figure. Therefore, we use dots for the simulation results, located in the middle of the interval.

A second limitation comes from the position where we detect the domain wall due to the time the domain wall needs to reach this position. At the beginning of the wire the x components are very small and can change their sign due to spin wave excitation, so we decided to detect the passing domain walls at the 20th lattice site after the last fixed magnetization. With a speed of more than 100m/s a domain wall reaches the 20th lattice site in less than 1ns so we can detect domain walls with a creation time of 99ns . The critical current densities in our simulation are in order of 10^{12} A/m^2 so the additional current density we need to create domain walls in less than 99ns is in the range of 0.2% of the critical current density.

To determine the critical current density via nested intervals we define an interval $\pm 1 \cdot 10^{12} \text{ A/m}^2$ around the theoretical value. So for the lower border j_{lower} of the interval there shall be no domain wall creation but for the higher border j_{higher} it should. We simulate the system as described in section 4.5 for both borders of the interval. If there is no domain wall creation for the lower border but for the higher border, we simulate the system again for the current strength in the middle of the interval $j_{\text{middle}} = (j_{\text{higher}} + j_{\text{lower}})/2$. If there is no domain wall creation for j_{middle} the critical current is between j_{middle} and j_{higher} . If a domain wall was created the value is between j_{middle} and j_{lower} . By this method we shrink the size of the interval down to $\sim 4\%$. Because of the critical current value depending on the ground state

4. Domain wall creation with DMI by STT

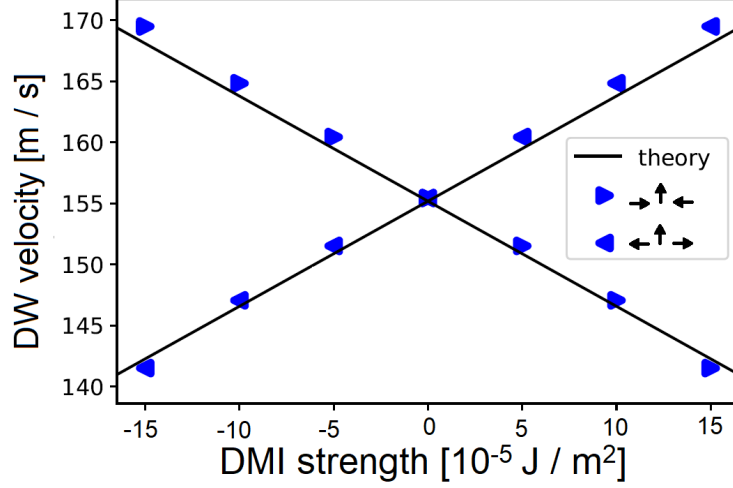


figure 4.5.: Simulation results for the velocities of both types of domain walls for different DMI strengths. The velocity has a linear dependence on the DMI strength but is different for both types of domain walls. While DMI increases the velocity for one type it decreases the speed of the other type.

we simulate the system for both ground states.

The simulation results are shown in figure 4.4. The simulation results are plotted as dots because the sizes of the intervals are too small to be seen in this figure. In comparison to our previous method this simulation results matches better to our analytic predictions.

4.5.3. Domain wall velocity and interaction

Another effect we discussed in our calculation is the domain wall velocity, and the interaction and annihilation of the domain walls.

To determine the speed of both types of domain walls we perform another simulation. We use a nanowire with 2048 lattice sites and create a domain wall at the 100th lattice site. We ramp up the current in $5ns$ so the domain wall has full speed at the 500th lattice site. We measured the time the domain wall needs to cover the distance from the 500th to 1500th lattice site. By dividing the distance by the time the domain wall needed for the distance we obtain the speed of the domain wall. We perform this simulation for both domain wall types and different DMI strengths.

The results are shown in figure 4.5. As in the theory part described (equation 4.23) the velocity of the domain wall depends linearly on the DMI strength for small values of

4. Domain wall creation with DMI by STT

D. Especially, the DMI increases the velocity of one type of domain wall and decreases the velocity of the other type. In the theory we have used a linear approximation for small DMI strengths, which is a possible explanation for the slightly increasing difference between theory and numerics for higher DMI strengths.

For the interaction we relax a state containing two domain walls separated by a distance of 100 lattice sites (300nm). The domain wall width is $\Delta = 36 \text{ nm}$ so the domain walls have a large separation. We drive the domain walls by applying a current of $2.5 \cdot 10^{11} \text{ A/m}^2$ current. The position of each domain wall is obtained by linear interpolation of the x components of the magnetizations, where the sign of the x components changes

$$X_{1,2} = -\frac{M_x[i]}{M_x[i+1] - M_x[i]} + x[i] \quad (4.31)$$

where i is the number of the magnetization, $x[i]$ the position of the magnetization, $M_x[i]$ the x component of the magnetization and the sign of $M_x[i]$, and $M_x[i+1]$ is different.

In figure 4.6 there are the simulation results for different DMI strength. The graphics show the time dependence of the distance between the two domain walls and of the relative angle between them. If the front domain wall is the faster one the distance increases and by this the interaction decreases (figure 4.6 (a)). For a set-up without DMI the domain wall velocity is equal for both types (b). There is only a small interaction between them which effect an oscillation of the separation distance between the domain walls. The mean separation distance is constant.

For a set-up where the front domain wall is the slower one the distance between the domain walls decreases in time. By this the interaction becomes stronger which can be observed by the increasing amplitude of the oscillation. In contrast to the system without DMI the mean separation distance decreases in time. At some point the attractive interaction is too strong and the domain walls annihilate. For increasing DMI strengths the annihilation process takes place earlier. For very weak DMI strength, the interaction of the domain walls is for a longer time observably. Figure 4.7 shows the interaction in a wire with a weak DMI strength of $1 \cdot 10^{-5} \text{ J/m}^2$.

4. Domain wall creation with DMI by STT

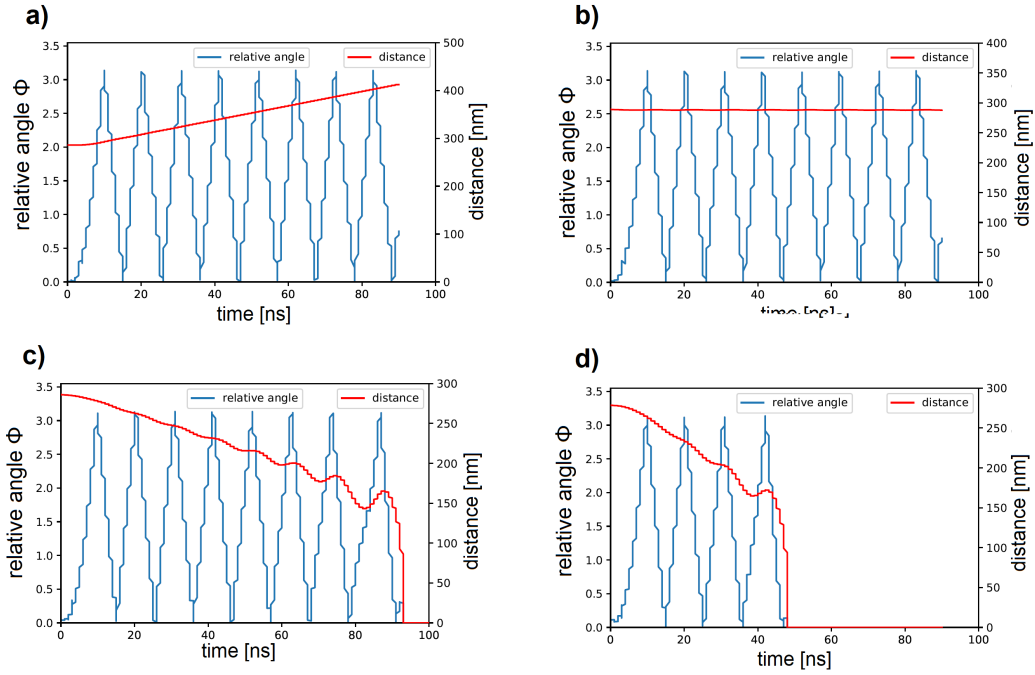


figure 4.6.: The figures show the distance and the relative angle between two domain walls during their movement in a wire. a) shows a set-up with a DMI strength of $5 \cdot 10^{-5} J/m^2$ where the previous domain wall is the faster one so the distance increase in time. b) shows a set-up without DMI so both domain walls move with the same velocity. c) shows the results from a set-up with a DMI strength of $5 \cdot 10^{-5} J/m^2$ but the previous domain wall is the slower one. The distance decreases, the interaction becomes stronger and at some point the domain walls annihilate. d) shows the results of the same set-up like c) but with a DMI strength of $10 \cdot 10^{-5} J/m^2$. The difference of the velocities is bigger and the annihilation happens earlier. c) and d) show both that whether the interaction is attractive or repulsive depends on relative angle.

4. Domain wall creation with DMI by STT

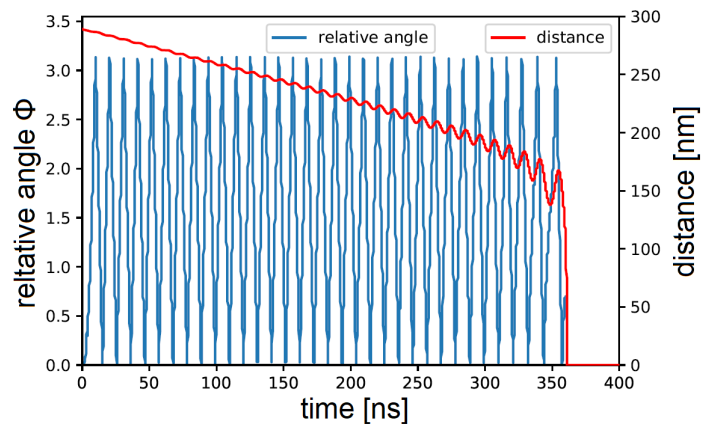


figure 4.7.: The interaction between two domain walls in a wire with a DMI strength of $1 \cdot 10^{-5} J/m^2$. The front domain wall is slower so the distance between the domain wall decreases. Due to the small DMI strength the interaction is observable for a long time. The interaction becomes stronger if the distance shrinks. Whether the interaction is attractive or repulsive strongly depends on the relative angle between the domain walls.

5. Domain wall creation without Dzyaloshinskii-Moriya interaction by spin orbit torques

In this chapter we investigate the creation of domain walls by spin orbit torques (SOT). This chapter is divided into a theory part and a simulation part. In the first part we present our analytic calculations. The calculations are very similar to the calculations of the critical current in chapter 4 so we present now only the main steps. In the second part we compare our analytic results to micromagnetic simulations.

5.1. Critical current without DMI

In this section we analyze the domain wall creation by spin orbit torques in a system without DMI (only exchange and anisotropy). The spin orbit torque effects a change of the magnetization perpendicular to the magnetization direction and the spin polarization $\boldsymbol{\sigma}$. If the spin polarization $\boldsymbol{\sigma}$ is not parallel to the $\hat{\boldsymbol{x}}$ direction the SOT acts a torque on the ground state of the system so the ground state is not independent from the current. Due to this reason we choose $\boldsymbol{\sigma} \parallel \hat{\boldsymbol{x}}$. More precisely,

$$\boldsymbol{\sigma} = \hat{\boldsymbol{z}} \times \boldsymbol{j} \quad (5.1)$$

with $\boldsymbol{j} = -j\hat{\boldsymbol{y}}$.

To calculate the critical current value for domain wall creation with SOT we use the same method as in section 4. To find the first conserved quantity we use the LLG without damping terms

$$\dot{\boldsymbol{m}} = -\gamma \boldsymbol{m} \times \boldsymbol{H}_{\text{eff}} - \tau_{\text{FL}} (\boldsymbol{m} \times \boldsymbol{\sigma}) . \quad (5.2)$$

With

$$\boldsymbol{H}_{\text{eff}} = \frac{1}{M_s} \left(J \partial_x^2 \boldsymbol{m} + 2\lambda M_x \hat{\boldsymbol{x}} \right) \quad (5.3)$$

and equation 5.1 we can rewrite the LLG for a one dimensional wire

$$\begin{aligned} \dot{m}_x &= -\frac{\gamma}{M_s} J \hat{\boldsymbol{x}} \left(\boldsymbol{m} \times \partial_x^2 \boldsymbol{m} \right) - \tau_{\text{FL}} j \hat{\boldsymbol{x}} \cdot (\boldsymbol{m} \times \hat{\boldsymbol{x}}) \\ &= -\partial_x \left(\frac{\gamma}{M_s} J \hat{\boldsymbol{x}} (\boldsymbol{m} \times \partial_x \boldsymbol{m}) \right) = 0 . \end{aligned}$$

5. Domain wall creation without DMI by SOT

At the critical point the system changes from the stable to the unstable state so we calculate for what values of τ_{FL} the system is still stable. For $\dot{m}_x = 0$ the derivative in the above equation is equal to zero so the argument in the brackets is a constant. We can calculate this constant at $x \rightarrow \infty$ where $\partial_x \mathbf{m} = 0$ and $m_x = 1$ and we obtain

$$\partial_x m_y = 0. \quad (5.4)$$

We can rewrite the LLG (equation (5.2)) to a more general form

$$\dot{\mathbf{m}} = \frac{\gamma}{M_s} \mathbf{m} \times \frac{\delta F_{\text{eff}}[\mathbf{m}, \tau_{\text{FL}}]}{\delta \mathbf{m}} \quad (5.5)$$

with

$$F_{\text{eff}}[\mathbf{m}, \tau_{\text{FL}}] = \int_0^\infty dx \left[\frac{J}{2} (\partial_x \mathbf{m})^2 + \lambda (1 - m_x^2) - \frac{\tau_{\text{FL}} M_s}{\gamma} \mathbf{m} \cdot \boldsymbol{\sigma} \right]. \quad (5.6)$$

The physical solution will minimize $F_{\text{eff}}[\mathbf{m}, \tau_{\text{FL}}]$ so we interpret $F_{\text{eff}}[\mathbf{m}, \tau_{\text{FL}}]$ again as action with x as time and we obtain as Lagrangian and corresponding Hamiltonian

$$\mathcal{L} = \frac{J}{2} (\partial_x \mathbf{m})^2 + \lambda (1 - m_x^2) - \frac{\tau_{\text{FL}} M_s}{\gamma} \mathbf{m} \cdot \boldsymbol{\sigma} \quad (5.7)$$

$$\mathcal{H} = \frac{J}{2} (\partial_x \mathbf{m})^2 - \lambda (1 - m_x^2) - \frac{\tau_{\text{FL}} M_s}{\gamma} \mathbf{m} \cdot \boldsymbol{\sigma}. \quad (5.8)$$

The Hamiltonian is conserved because it does not depend explicitly on the "time" x . We can calculate the value of the Hamiltonian at $x \rightarrow \infty$ and with $\boldsymbol{\sigma} = j \hat{x}$

$$\frac{J}{2} (\partial_x \mathbf{m})^2 - \lambda (1 - m_x^2) - \frac{\tau_{\text{FL}} M_s}{\gamma} \mathbf{m} \cdot \boldsymbol{\sigma} = -\frac{\tau_{\text{FL}} M_s}{\gamma} j. \quad (5.9)$$

At the beginning of the wire where $\mathbf{m} = \hat{z}$ equation (5.9) gives

$$(\partial_x \mathbf{m})^2 = \frac{2}{J} \left(\lambda - \frac{\tau_{\text{FL}} M_s j}{\gamma} \right) \quad (5.10)$$

Using that at the fixed magnetization $(\partial_x \mathbf{m})^2 = (\partial_x m_x)^2 + (\partial_x m_y)^2$ and the equations (5.4) and (5.10) we get

$$(\partial_x m_x)^2 = (\partial_x \mathbf{m})^2 - (\partial_x m_y)^2 = \frac{2}{J} \left(\lambda - \frac{\tau_{\text{FL}} M_s j}{\gamma} \right) \geq 0. \quad (5.11)$$

If the current density is equal to the critical value $j = j_c$ the above expression has to be equal to zero. From this follows

$$\tau_{\text{FL}} = \frac{\gamma \lambda}{M_s j_c}. \quad (5.12)$$

5. Domain wall creation without DMI by SOT

We can also calculate τ_{FL} from material parameters [35, 46]

$$\tau_{\text{FL}} = \frac{\gamma\xi\hbar\theta_{\text{Hall}}}{2M_s e t} \quad (5.13)$$

where t is the thickness of the ferromagnetic layer, θ_{Hall} the constant of the spin Hall effect and $\xi = \frac{\tau_{\text{FL}}}{\tau_{\text{DL}}}$ the ratio of the constants from the field like term and the damping like term. ξ and θ_{Hall} are material dependent parameters. For the other ground state $\mathbf{m} = -\hat{\mathbf{x}}$ the result for τ_{FL} has the opposite sign.

With the both expressions for τ_{FL} 5.12 and 5.13 we calculate our critical current density

$$j_c = \frac{2\lambda e t}{\xi\hbar\theta_{\text{Hall}}}. \quad (5.14)$$

In our calculations we assume $\tau_{\text{DL}} = 0$. For $\tau_{\text{DL}} \rightarrow 0$ the ratio $\xi \rightarrow \infty$ and by this the critical current vanishes $j_c \rightarrow 0$. Especially, for $\xi \rightarrow 0$ where the field like term vanishes our theoretical result for j_c diverges $j_c \rightarrow \infty$. So our result should be only valid for a dominant field like term $\xi \gg 1$.

5.2. Simulation

The spin orbit torque with spin polarization $\boldsymbol{\sigma}$ in $\hat{\mathbf{x}}$ direction effects a rotation of the domain wall around the wire but no movement of the wall. The direction of the rotation is defined by the sign of τ_{FL} and by the type of domain wall. So one domain wall type rotates clock wise the other one counter clock wise. However, the torque does not move the domain wall. In this case the Gilbert damping $\alpha \mathbf{m} \times \dot{\mathbf{m}}$ term can move the domain wall. The movement is perpendicular to the magnetization and the change of the magnetization direction $\dot{\mathbf{m}}_{\text{mov}} \parallel \mathbf{m} \times \dot{\mathbf{m}}$. Hence, for a rotating domain wall the movement is along the $\hat{\mathbf{x}}$ axis. The direction of the movement depends on the direction of the rotation. Thus, the spin orbit torque moves domain walls in the opposite direction depending on their type.

Due to that reason there is no periodic domain wall creation possible, especially the domain wall creation stops after one domain wall was created. Therefore we use the method of nested intervals (like it was described in the previous chapter) to analyze for what current densities there is domain wall creation. We perform the simulation for several values of ξ and without DMI. For all the other constants we use the same values given in the table in section 4.5.

Our results are shown in figure 5.1. Our theory diverges if $\xi \rightarrow 0$ but the simulation results goes to $2.23 \cdot 10^{10} \text{A/m}^2$ for $\xi = 0$. For $\xi \gg 1$ the simulation results and our theory approaches.

5. Domain wall creation without DMI by SOT

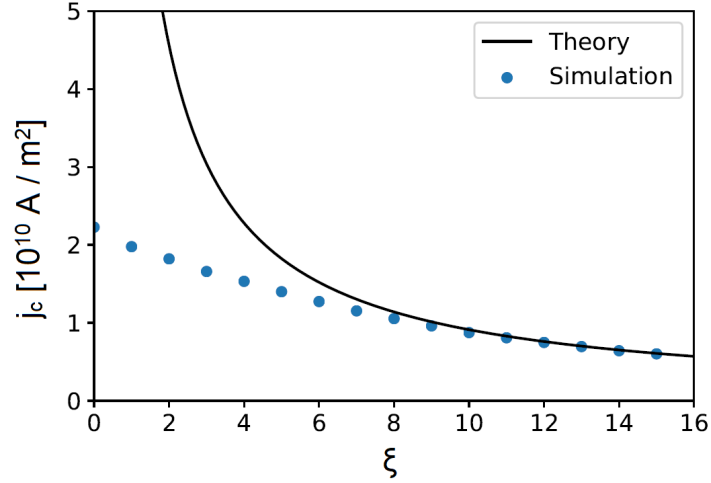


figure 5.1.: Simulation results and theory of the critical current density for domain wall creation by spin orbit torques for different values of ξ . For a dominant field like term $\xi \gg 1$ the simulation results fit well with the theoretical prediction. For small values of ξ the theory diverges but the simulation results remain in the same order of magnitude.

Our theory predicted that the critical current depends linear on the anisotropy strength λ but is independent of the exchange constant J . We simulate the system for different values of λ and J once for a high value of $\xi = 15$ and once for $\xi = 0$. For $\xi = 0$ we do not have any theoretical predictions. The results are shown in figure 5.2. The simulations show that the critical current is independent of the exchange constant. For the set-up with a large ξ the result fit with the theory. For $\xi = 0$ the critical current is also constant except some fluctuations. The simulation for the different anisotropy values shows a linear dependence for both simulation $\xi = 15$ and $\xi = 0$. For the large ξ the results goes with our theory.

5. Domain wall creation without DMI by SOT

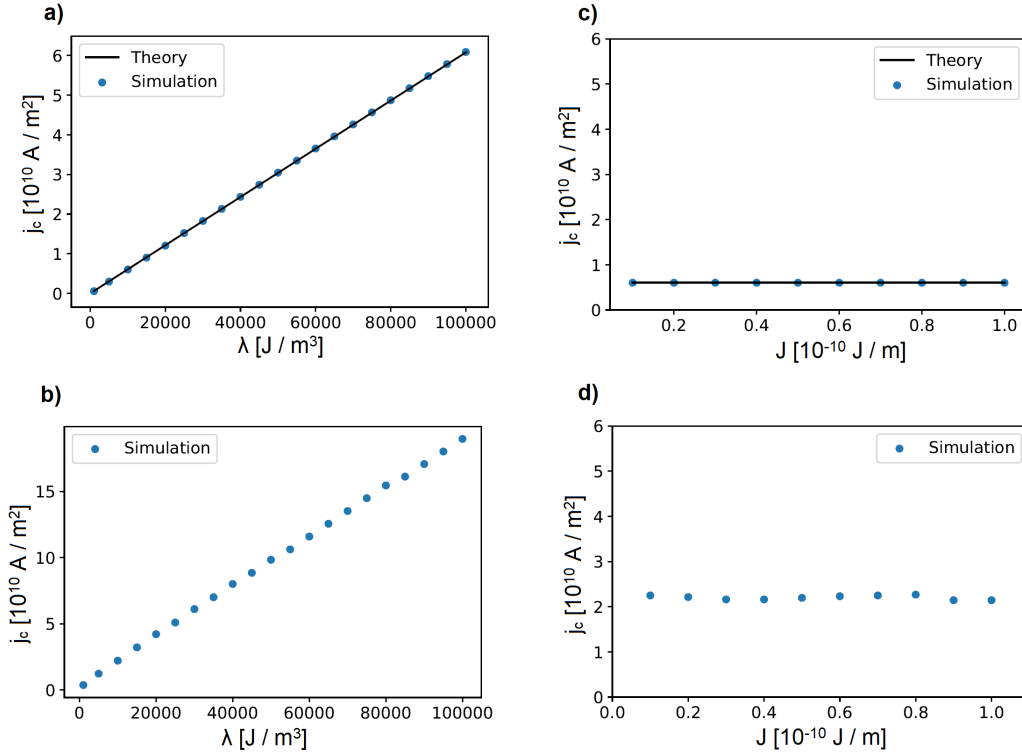


figure 5.2.: a) and b) shows the critical current density for different values of the anisotropy constant λ . In a) the ratio $\xi = 15$ and the simulations fits with the theoretical predictions. For $\xi = 0$ b) our theory diverges so there are only results from the simulation. The simulation shows also a linear dependence. In c) and d) is the critical current for different values of the exchange constant J . c) is a simulation with a large ratio of $\xi = 15$ and d) is simulated with $\xi = 0$. In both cases the critical current density is independent of J and for the large ξ it fits with our theory.

6. Domain wall creation with Dzyaloshinskii-Moriya interaction by spin orbit torques

In this chapter we analyze the effect of additional Dzyaloshinskii-Moriya interaction to the domain wall creation by SOT.

6.1. Critical current with DMI

We consider the same set-up like in chapter 4, a nanowire with exchange interaction, anisotropy and DMI but the domain wall creation works by SOT. The energy is given by (2.13) and the effective magnetic field is given by (4.8). The LLG reads

$$\begin{aligned}\dot{m}_x &= -\frac{\gamma}{M_s} \left(J\hat{\mathbf{x}} \cdot (\mathbf{m} \times \partial_x^2 \mathbf{m}) - 2D(m_z \partial_x m_z - m_y \partial_x m_y) \right) - \tau_{\text{FL}} j \hat{\mathbf{x}} \cdot (\mathbf{m} \times \hat{\mathbf{x}}) \\ &= \partial_x \left(-\frac{\gamma}{M_s} \left(J\hat{\mathbf{x}} \cdot (\mathbf{m} \times \partial_x \mathbf{m}) - Dm_x^2 \right) \right) = 0.\end{aligned}$$

The argument in the brackets is a constant which we can calculate again for $x \rightarrow \infty$. We obtain

$$\partial_x m_y = \frac{D}{J}. \quad (6.1)$$

We use the general form of the LLG without Damping terms

$$\dot{\mathbf{m}} = \gamma \mathbf{m} \times \frac{\delta F_{\text{eff}}[\mathbf{m}, \tau_{\text{FL}}]}{\delta \mathbf{m}} \quad (6.2)$$

and get the same conserved Hamiltonian as in the previous chapter

$$\mathcal{H} = \frac{J}{2} (\partial_x \mathbf{m})^2 - \lambda (1 - m_x^2) - \frac{\tau_{\text{FL}} M_s}{\gamma} \mathbf{m} \cdot \boldsymbol{\sigma} = -\frac{\tau_{\text{FL}} M_s}{\gamma} j. \quad (6.3)$$

From the Hamiltonian we get

$$(\partial_x \mathbf{m})^2 = \frac{2}{J} \left(\lambda - \frac{\tau_{\text{FL}} M_s j}{\gamma} \right). \quad (6.4)$$

With $(\partial_x \mathbf{m})^2 = (\partial_x m_x)^2 + (\partial_x m_y)^2$ we can calculate τ_{FL} for the critical current density

6. Domain wall creation with DMI by SOT

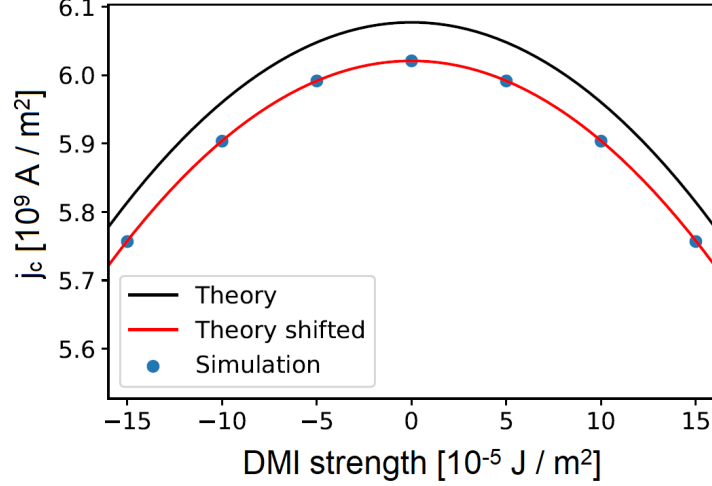


figure 6.1.: Simulation results for the critical current density for domain wall creation by spin orbit torques in a wire with DMI. The blue dots are the critical current density determined by the method of nested intervals. The difference between theory simulation and theoretical predictions is in the same order like previous simulation results. They are viable due to the different zoom factor (y axis). The red line is the shifted theory. It is shifted to the simulation result without DMI. The slope of theory and simulation is similar.

j_c

$$\tau_{\text{FL}} = \frac{\gamma}{j_c} \left(\lambda - \frac{D^2}{2J} \right). \quad (6.5)$$

With equation 5.13 we get a value for the critical current density

$$j_c = \frac{2et}{\xi \hbar \theta_{\text{Hall}}} \left(\lambda - \frac{D^2}{2J} \right). \quad (6.6)$$

For $D = 0$ we obtain the result for the critical current density we calculated in the previous chapter (equation (5.14)). Our results show a quadratic decreasing of the critical current density with increasing DMI strength. Hence, the critical current density does not depend on the sign of the DMI and in comparison to the chapter of domain wall creation by spin transfer torques (chapter 4) there is no symmetry breaking due to DMI.

6.2. Simulation

For the simulation of the domain wall creation by spin orbit torques in a wire with DMI we use the parameters from section 4.5. To determine the critical current we use the method of nested intervals.

The results are shown in figure 6.1. The critical current has a parabolic shape. DMI decreases the critical current density quadratic so it is symmetric around its maximum at $D = 0$.

7. Conclusion and outlook

In this thesis we investigated the domain wall creation at a pinned 90 degree domain wall by spin transfer torques and spin orbit torques. We had a special interest on the critical current density which is needed to create domain walls. We expanded the theoretical predictions of reference [11] by adding Dzyaloshinskii-Moriya interaction and spin orbit torques to the system. We showed that DMI can decrease the critical current density and it depends linear on the DMI strength. Furthermore, DMI breaks the symmetry of both possible types of domain walls (head to head and tail to tail). By decreasing the critical current density for the creation of the one type of domain wall, it increases the critical current density for the other type. This causes additionally a different creation time of both types, so one type is created faster than the other one.

Further, we showed that DMI has an effect on the behavior of the domain walls after their creation. Due to their different creation time, their different velocities and the interaction between each other the domain walls annihilate. We showed that with increasing DMI strength the annihilation process happens earlier in the wire.

In the second part of the thesis we analyzed the creation of domain walls by spin orbit torques. We found that the critical current density is independent of the strength of exchange interaction and depends linear on the anisotropy constant. DMI decreases the critical current density quadratically and especially there is no symmetry breaking due to DMI for the creation via spin orbit torques.

We performed micro magnetic simulation and compare the results to our analytic calculation. For the determination of the critical current density we used two methods (frequency method and nested intervals). Additionally we determined the speed of both types of domain walls by the simulation and showed that they depend linear on the DMI strength. We observed the interaction and annihilation of two domain walls in the wire and showed that they depend mainly on the relative angle between them.

While we neglected the damping like terms in our calculations we had to add them to our simulation. In particular, the simulation results for the domain wall creation via spin orbit torques showed a significant influence of the damping like terms on the critical current density. Furthermore, we assumed for the spin orbit torques a spin current polarization along the wire what corresponds to an electric current flowing perpendicular to it. The investigation of the influence of the damping like terms and the possibility of domain wall creation by spin orbit torques with a spin polarization perpendicular to the wire may be of interest for further research.

Abbildungsverzeichnis

2.1. Bloch and Néel type domain wall	5
2.2. Head to head, tail to tail domain walls and soft modes	6
2.3. Spin transfer torque and spin orbit torque	7
2.4. Movement of a domain wall by spin transfer torque	9
2.5. Different ground state of the nanowire for different DMI strengths . .	10
2.6. The two ground states of the nanowire	11
3.1. set-up of a ferromagnetic nanowire	13
4.1. Peridoc Domain wall creation in ferromagnetic wire with DMI	19
4.2. Determination of j_c for a fixed DMI strength	23
4.3. Simulation result of the domain wall creation with STT and frequency method	24
4.4. Simulation result of the domain wall creation with STT and nested interval method	25
4.5. Velocity of both types of domain walls for different DMI strengths. . .	26
4.6. Distance and relative angle of two domain walls during annihilation in a set-up for different DMI	28
4.7. Distance and relative angle of two domain walls during annihilation in a set-up with small DMI	29
5.1. Simulation results of domain wall creation by spin orbit torques in a wire without DMI	33
5.2. Simulation results for the domain wall creation by SOT for different values of anisotropy and exchange constant	34
6.1. Simulation results for the domain wall creation by spin orbit torques in a wire with DMI	36
A.1. Determination process of the critical current by the frequency method	41
A.2. Magnetization dynamic of the 50th lattice site after the last fixed magnetization for different DMI strengths	42
A.3. Determination of the critical current density for different DMI strength for both domain wall types	43
A.4. Results of the critical current determination by frequency method at different positions	44

A. Appendix

A.1. Nomenclature

DMI Dzyaloshinskii-Moriya interaction

LLG Landau-Lifshitz-Gilbert equation

STT Spin transfer torque

SOT Spin orbit torque

A.2. Additional figures

The following figures show the determination process for the critical current with the frequency method. The first figure A.1 is chart which shows the expiration of the process. The next two figures A.2, A.3 show the two different steps of the determination process for the different DMI strengths. The last figure A.4 shows the result of the determination at different lattice sites (50, 75, 100 and 100 lattice sites behind the fixed magnetization).

A. Appendix

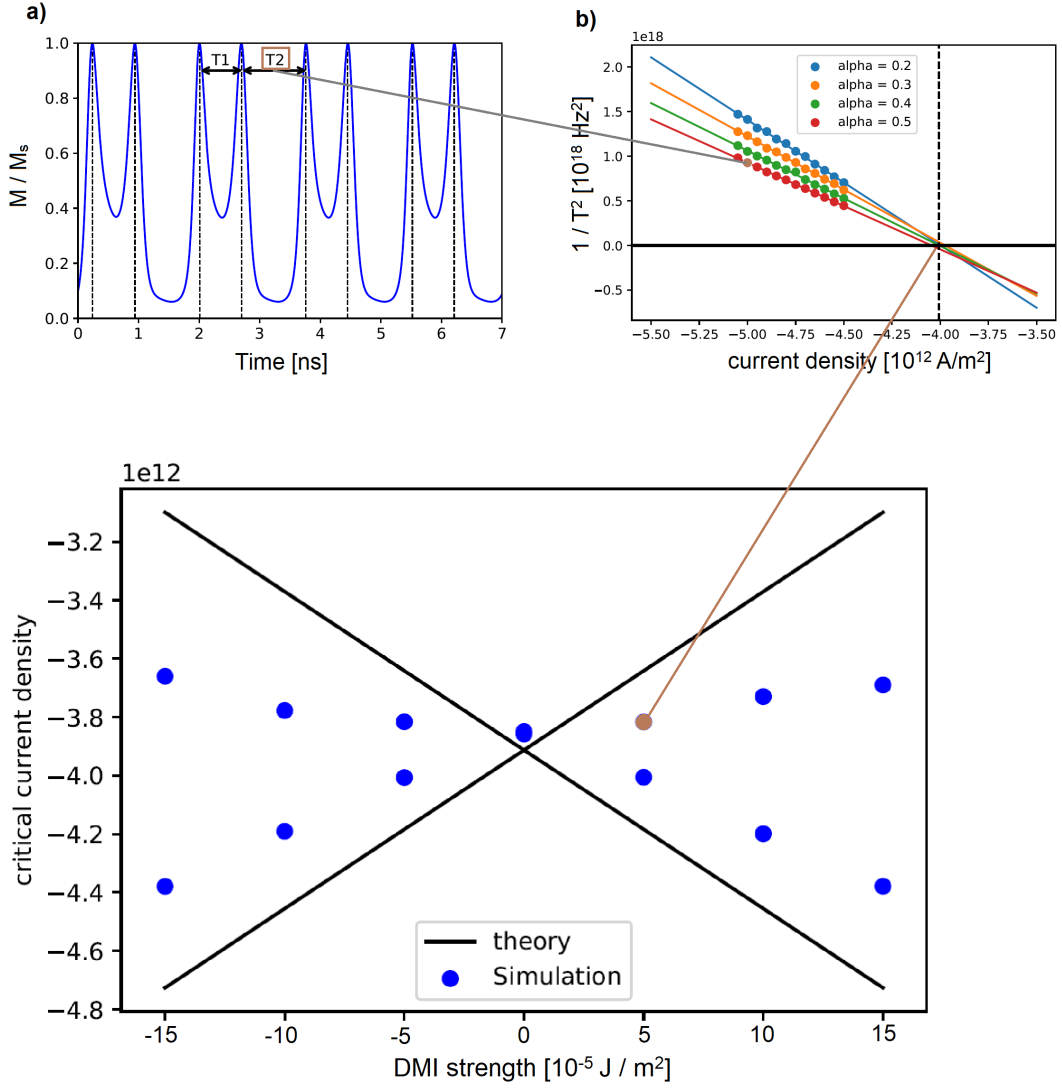


figure A.1.: Determination process of the critical current by the frequency method. First the two creation periods are determined by the dynamics of the magnetization 50 lattice sites after the last fixed magnetization. All periods for one DMI strength and one domain wall are squared. The inverted squared periods are plotted versus the current density and fitted by a line for each value of α separately. The crossing point with the x axis represents the critical current density. The mean value of all four results is the simulation result of the critical current density for this domain wall type and DMI strength.

A. Appendix

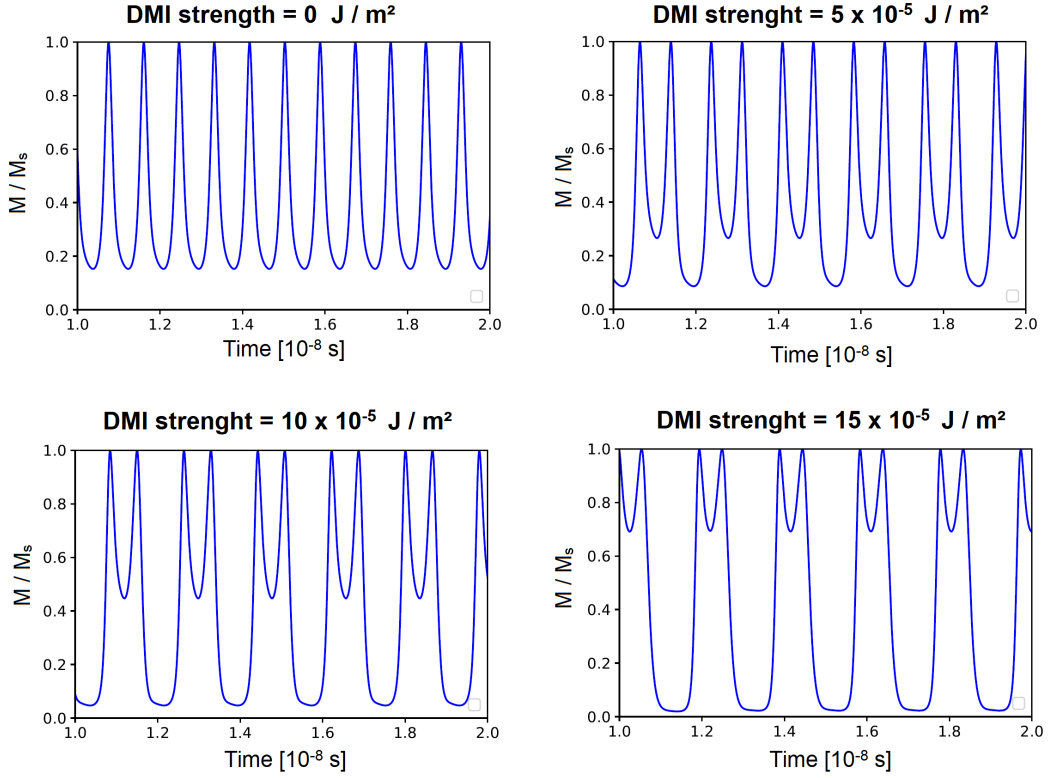


figure A.2.: Magnetization dynamic of the 50th site after the last fixed magnetization for different DMI strengths and a current density of $5 \cdot 10^{12} \text{ A/m}^2$. The figure in the upper left shows the domain wall creation without DMI. The creation frequency for both domain wall types is the same so the creation is symmetric. Due to a small creation time the initial domain wall distance is smaller than the domain wall width Δ , so the perpendicular component of the magnetization do not has its minimum at 0. The following figures show the domain wall creation in a system with DMI. The stronger the DMI the bigger is the difference between the creation times.

A. Appendix

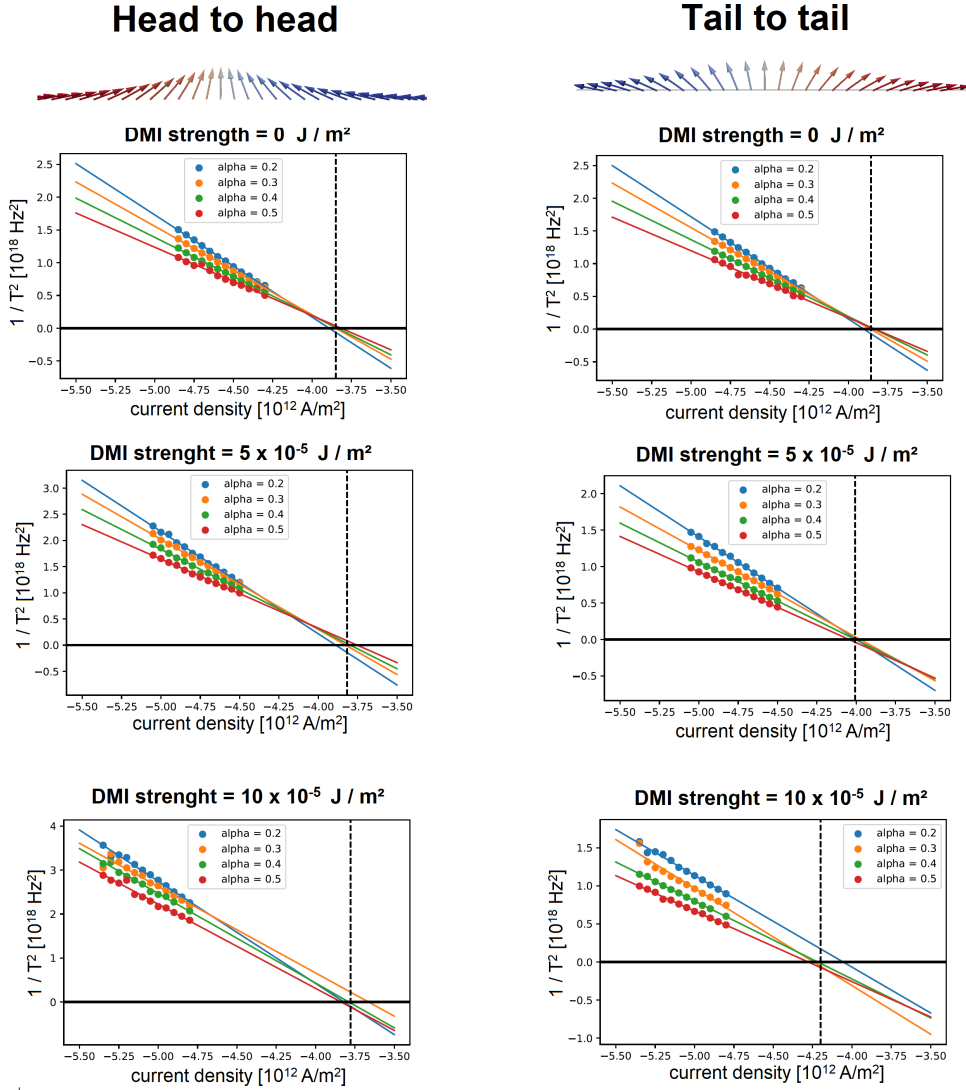


figure A.3.: Determination of the critical current density for different DMI strength for both domain wall types. On the left side there are the results for the head to head domain wall on the right side the results for the tail to tail domain wall. Without DMI (first row) the critical current densities are the same for both types. For increasing DMI the critical current density increases for the tail to tail domain wall while it decreases for the head to head domain wall. Due to the higher creation frequency for, in this case, the head to head domain wall the simulation becomes more inaccurate what constitute the increasing difference between linear fit and simulation results.

A. Appendix

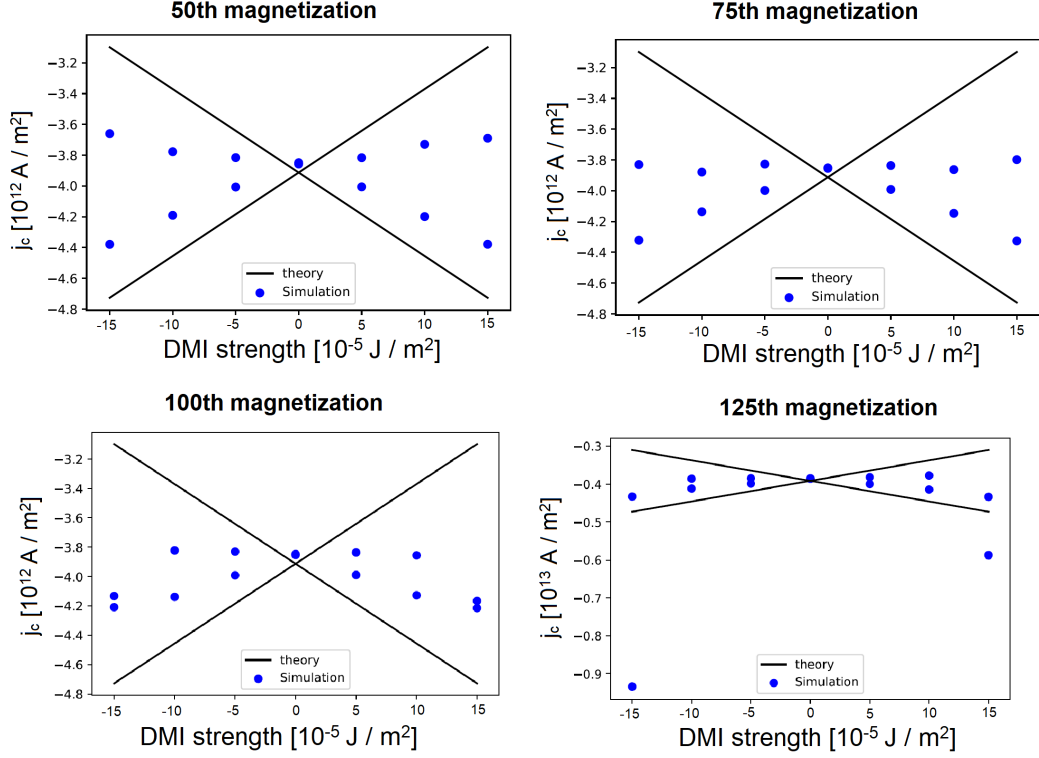


figure A.4.: Determination of the critical current by frequency method at different lattice sites. The results of the simulation of the magnetizations 50, 75, 100 and 125 lattice sites behind the last fixed magnetization are shown. The critical current value differs from the theoretical predictions due to interaction between the domain walls during their movement to the magnetization where the dynamics are analyzed. The simulation results of the several magnetization differs also due to this interaction.

A.3. Numeric Simulation Codes

The python code where we define our material for our numeric simulation. The code was originally written by Matthias Sitte and Karin Everschor-Sitte for the numeric simulations for the paper [11] and was edited by Nils Sommer for the simulation for this thesis.

The following pages show the main parts of the simulation code.

1. Relaxation process
2. Simulation with current ramp up
3. Determination of the frequency for the frequency method
4. Main loop for the frequency method
5. Determination if a domain wall was created for the nested intervals method
6. Main loop for the nested intervals method

```

def compute_relaxed_groundstate(alpha, dmi, force_relax=False):
    """Compute the relaxed groundstate of the nanowire with pinned impurity
    site without applied electric current.

    Args:
        alpha (float): The Gilbert damping parameter.
        force_relax (boolean): Flag whether to force the computation of the
            relaxed groundstate even if it has already been computed.

    Returns:
        The file name and path for the relaxed groundstate.
    """
    # Define the file name and path for the relaxed groundstate.
    outfile = "nanowire_relaxed_len={0}_BDMI={1}_M.ovf".format(XNODES, dmi)
    basename = os.path.splitext(os.path.abspath(outfile))[0]

    # Check if the relaxed magnetization has been computed in an earlier run.
    # If the output file exists, the calculation is not redone *unless* the
    # user uses the "--force-relax" flag.
    if os.path.exists(outfile) and not force_relax:
        print('(II) Relaxed state already computed. Nothing to do here ...')
        return outfile

    # Create the mesh with open boundary conditions.
    mesh = RectangularMesh((XNODES, YNODES, ZNODES),
                           (XSTEPsize, YSTEPsize, ZSTEPsize),
                           periodic_bc='')

    # Create the material for the nanowire.
    material_nanowire = Material({
        'id': 'nanowire',
        'Ms': SATURATION_MAGNETIZATION,
        'A': EXCHANGE_COUPLING,
        'alpha': alpha,
        'axis1': UNIAXIAL_ANISOTROPY_DIRECTION,
        'k_uniaxial': UNIAXIAL_ANISOTROPY_STRENGTH
    })

    # Create simulation 'world'.
    body_nanowire = Cuboid((0, 0, 0), (XNODES, YNODES, ZNODES))
    nanowire = Body('nanowire', material_nanowire, body_nanowire)
    world = World(mesh, nanowire)

    # Create a solver to relax the magnetization taking into account exchange
    # interaction, anisotropy, and local pinning field.
    solver = create_solver(
        world, [ExchangeField, AnisotropyField, DMIField, ExternalField], log=True)

    #add DMI
    dx_dmi = (-dmi,0,0)
    dy_dmi = (-dmi,0,0)
    solver.state.Dx.fill(dx_dmi)
    solver.state.Dy.fill(dy_dmi)

    # Apply local magnetic field to impurity site.
    solver.state.H_ext_fn = lambda time: pinning_field(mesh, time)

    # Initialize the magnetic state.
    for i in range(0, LAST_FIXED_MAG):
        solver.state.M.set(i, 0, 0, INITIAL_STATE_IMPURITY)
    for i in range(LAST_FIXED_MAG, XNODES):

```

```

    solver.state.M.set(i, 0, 0, INITIAL_STATE_NANOWIRE)

# Create a step handler which stores the magnetization every 1/100th of a
# nanosecond.
# NB: The step handler automatically creates the directory `workdir` if it
# does not exist. Existing files in the directory will be overwritten
# without notification.
workdir = basename + '.run'
solver.addStepHandler(
    OOMMFStorage(workdir, 'M', omf_format=OMF_FORMAT_BINARY_8),
    condition.EveryNthSecond(1.0e-11))
#solver.addStepHandler(
#    VTKStorage(workdir, 'M'),
#    condition.EveryNthSecond(1.0e-10))

# Set up the log file.
# NB: `log` must be an open file object.
logfile = basename + '.log'
try:
    log = open(logfile, 'w')
except:
    print('(EE) Failed to open log file!')
    raise # throw again to let the caller know what happened

solver.addStepHandler(FileLog(log), condition.EveryNthStep(100))

# Relax state -- this will find the nearest (metastable) state with lowest
# energy (which is not necessarily the true ground state of the system).
solver.solve(condition.Relaxed(1))

# Finally write the relaxed magnetization profile to the OVF output file.
writeOMF(outfile, solver.state.M, format=OMF_FORMAT_BINARY_8)

# Close the log file.
log.close()

return outfile

```

```

def run_simulation(alpha, j0, j1, tau, time, infile, dmi, force_sim=False):
    """Apply a current ramp from `j0` to `j1` with a sinusoidal function in
    ramp time `tau`.

    Args:
        alpha (float): The Gilbert damping parameter.
        j0 (float): The initial current strength.
        j1 (float): The target current strength.
        tau (float): The current ramp time.
        infile (str): File name and path containing the initial state.
        force_rsim (boolean): Flag whether to force the run of the simulation
            even if it already ran before.

    Returns:
        The file name and path for the magnetization at the end of the
        simulation.
    """
    # Define the file name and path for the magnetization at the end of the
    # simulation.
    outfile = "nanowire_shedding_len={0}_j0={1}_j1={2}_tau={3}_alpha={4}_BDMI={5}" \
        "_M.ovf".format(XNODES, j0, j1, tau, alpha, dmi)
    basename = os.path.splitext(os.path.abspath(outfile))[0]

    # Check if the simulation has been run before. If the output file exists,
    # the calculation is not redone *unless* the user uses the "--force-sim"
    # flag.
    if os.path.exists(outfile) and not force_sim:
        print('(II) Simulation already run. Nothing to do here ...')
        return outfile

    # Create the mesh with open boundary conditions.
    mesh = RectangularMesh((XNODES, YNODES, ZNODES),
                           (XSTEPsize, YSTEPsize, ZSTEPsize),
                           periodic_bc=' ')

    # Create the material for the nanowire.
    material_nanowire = Material({
        'id': 'nanowire',
        'Ms': SATURATION_MAGNETIZATION,
        'A': EXCHANGE_COUPLING,
        'alpha': alpha,
        'axis1': UNIAXIAL_ANISOTROPY_DIRECTION,
        'k_uniaxial': UNIAXIAL_ANISOTROPY_STRENGTH,
        'ST_p': CURRENT_SPIN_POLARIZATION
    })

    # Create simulation 'world'.
    body_nanowire = Cuboid((0, 0, 0), (XNODES, YNODES, ZNODES))
    nanowire = Body('nanowire', material_nanowire, body_nanowire)
    world = World(mesh, nanowire)

    # Create a solver to relax the magnetization taking into account exchange
    # interaction, anisotropy, and local pinning field.
    solver = create_solver(
        world, [ExchangeField, AnisotropyField, DMIField, ExternalField,
               SpinTorque, AlternatingCurrent],
        log=True)

    #add DMI
    dx_dmi = (-dmi,0,0)
    dy_dmi = (-dmi,0,0)

```

```

solver.state.Dx.fill(dx_dmi)
solver.state.Dy.fill(dy_dmi)

# Apply local magnetic field to impurity site.
solver.state.H_ext_fn = lambda time: pinning_field(mesh, time)

# Apply a time-dependent current.
solver.state.j_fn = lambda time: current_ramp_function(time, j0, j1, tau)

# Load the pre-computed magnetic state.
if not os.path.exists(infile):
    print("(EE) Can't find initial state: `{0}`".format(infile))
    sys.exit(1)
solver.state.M = readOMF(infile)

# Create a step handler which stores the magnetization every 1/10th of a
# nanosecond.
# NB: The step handler automatically creates the directory `workdir` if it
# does not exist. Existing files in the directory will be overwritten
# without notification.
workdir = basename + '.run'
solver.addStepHandler(
    OOMMFStorage(workdir, 'M', omf_format=OMF_FORMAT_BINARY_8),
    condition.EveryNthSecond(1.0e-10))
#solver.addStepHandler(
#    VTKStorage(workdir, 'M'),
#    condition.EveryNthSecond(1.0e-10))

# Set up the log file.
# NB: `log` must be an open file object.
logfile = basename + '.log'
try:
    log = open(logfile, 'w')
except:
    print('(EE) Failed to open log file!')
    raise # throw again to let the caller know what happened

solver.addStepHandler(FileLog(log), condition.EveryNthStep(100))

# Run the actual simulation.
runtime = tau + time
solver.solve(condition.Time(runtime))

# Finally write the relaxed magnetization profile to the OVF output file.
writeOMF(outfile, solver.state.M, format=OMF_FORMAT_BINARY_8)

# Close the log file.
log.close()

return outfile

```

```

#method to determine the two creation times
def dft_analysis(alpha, j0, j1, tau, dmi):

    # Define the file name and path for the magnetization which should have
    # been created at the end of the simulation.
    outfile = "nanowire_shedding_len={0}_j0={1}_j1={2}_tau={3}_alpha={4}_BDMI={5}"\
              "_M.ovf".format(XNODES, j0, j1, tau, alpha, dmi)
    basename = os.path.splitext(os.path.abspath(outfile))[0]
    workdir = basename + '.run'

    # Check if the simulation has been run before.
    if not os.path.exists(outfile):
        print("(EE) Can't find previous simulation!")
        sys.exit(1)

    # Load data files.
    tmp = []
    for ovf_file in sorted(glob.glob(os.path.join(workdir, '*.omf'))):
        tmp.append(read_ovf(ovf_file))

    if len(tmp) == 0:
        print('Could not find any data sets for Fourier analysis!')
        sys.exit(1)

    # Convert into Numpy array, removing first 20 nanoseconds due to current
    # ramp.
    data = np.array(tmp[200:])

    # determine the perpendicular magnetization component of the 150th lattice site.
    data = (data.T)[150]
    t = np.linspace(0, 1e-10*len(data), len(data))
    Mperp = 1-data**2

    #find maxima
    maxima = []
    b = False
    minimum_found = False

    #find first a minimum to avoid maxima at the boundary
    for i in range(len(Mperp)-1):
        if Mperp[i] < Mperp [i+1] and minimum_found == False:
            minimum_found = True
        if Mperp[i] > Mperp[i+1] and b == False and minimum_found == True:
            maxima.append(t[i])
            b = True
        if Mperp[i] < Mperp[i+1] and minimum_found == True :
            b = False

    T1 = []
    T2 = []
    i = 0

    #determine the two creation times as differences between the maxima and
    #order them T1 < T2
    while i < len(maxima)-2:
        T1.append(maxima[i+1]-maxima[i])
        T2.append(maxima[i+2]-maxima[i+1])
        i = i+2
    T1 = np.mean(T1)
    T2 = np.mean(T2)
    if T1 > T2:
        tmp = T1
        T1 = T2

```

```
T2 = tmp

with open(basename + '_maxmode.txt', 'w') as outfile:
    outfile.write("{0:.8g}\t{1:.8g}\t{2:.8g}\t{3:.8g}\t{4:.8g}".format(
        alpha, dmi, j1, T1, T2))
```

```

#main loop for the simulation for the frequency method

for dmi in [-15e-05, -10e-05, -5e-05, 0, 5e-05, 10e-05, 15e-05]:
    # Compute initial groundstate without current. The precise value of
    # `alpha` is not relevant (choosing small values will only result in
    # longer simulation times).
    relaxed_state = compute_relaxed_groundstate(
        alpha=0.25, dmi=dmi, force_relax=args.force_relax)

    for alpha in [0.5, 0.3, 0.4, 0.2]:
        infile = relaxed_state
        j0 = 0
        j1start = -5.1e12
        for j1 in np.arange(j1start, j1start-0.4e12, -0.05e12):
            # Run the simulation
            print("(II) Running simulation for alpha={0} ramping from " \
                  "j0={1} to j1={2} ...".format(alpha, j0, j1))
            current_state = run_simulation(
                alpha=alpha, j0=j0, j1=j1, tau=CURRENT_RAMPTIME,
                time=SIMULATION_TIME, infile=infile, dmi=dmi,
                force_sim=args.force_sim)

            # Perform the Fourier analysis.
            print('(II) Performing Fourier analysis of simulation data to ' \
                  'find the frequency for domain wall shedding ...')
            dft_analysis(alpha=alpha, j0=j0, j1=j1, tau=CURRENT_RAMPTIME, dmi=dmi)

```

```

#method to determine if there was domain wall creation
def analysis(alpha, j0, j1, tau, dmi):

    # Define the file name and path for the magnetization which should have
    # been created at the end of the simulation.
    outfile = "nanowire_shedding_len={0}_j0={1}_j1={2}_tau={3}_alpha={4}_BDMI={5}"\
              "_M.ovf".format(XNODES, j0, j1, tau, alpha, dmi)
    basename = os.path.splitext(os.path.abspath(outfile))[0]
    workdir = basename + '.run'

    # Check if the simulation has been run before.
    if not os.path.exists(outfile):
        print("(EE) Can't find previous simulation!")
        sys.exit(1)

    # Load data files.
    tmp = []
    for ovf_file in sorted(glob.glob(os.path.join(workdir, '*.ovf'))):
        tmp.append(read_ovf(ovf_file))

    if len(tmp) == 0:
        print('Could not find any data sets for analysis!')
        sys.exit(1)
    # Convert into Numpy array
    data = np.array(tmp[:])

    # check if the x component changes it sign in time
    #if yes a domain wall passed the 120th lattice site
    #note to change the sign >,< for the other ground state
    data = (data.T)[120]
    for i in data:
        if i<0:
            return True
    return False

```

```

#Loop to find critical current densities for different DMI strength via
#method of nested intervals
for dmi in [-15e-05, -10e-05, -5e-05, 0.0, 5e-05, 10e-05, 15e-05]:

    #compute relaxed ground state
    relaxed_state = compute_relaxed_groundstate(
        alpha=0.25, dmi=dmi, force_relax=args.force_relax)

    #define values for simulation
    jc = jc_theory(dmi)
    delta = 1e12

    alpha = 0.1
    infile = relaxed_state
    j0 = 0
    j1higher = jc+delta
    j1lower = jc-delta
    j1mid = (j1higher+j1lower)/2

    # check if DW creation is in the chosen interval

    #run simulation for the higher border of the electrical current interval
    print("(II) Running simulation for alpha={0} ramping from " \
          "j0={1} to j1={2} ...".format(alpha, j0, j1higher))
    current_state = run_simulation(
        alpha=alpha, j0=j0, j1=j1higher, tau=CURRENT_RAMPTIME,
        time=SIMULATION_TIME, dmi = dmi, infile=infile,
        force_sim=args.force_sim)

    print('(II) Performing analysis of simulation data to ')

    #check if a domain wall was created
    #if not the higher border is to low
    #stop simulation
    if analysis(alpha=alpha, j0=j0, j1=j1higher, tau=CURRENT_RAMPTIME, dmi=dmi) == False:
        print('No DW Creation in the chosen interval')
        return

    #run simulation for the lower border of the electrical current interval
    print("(II) Running simulation for alpha={0} ramping from " \
          "j0={1} to j1={2} ...".format(alpha, j0, j1lower))
    current_state = run_simulation(
        alpha=alpha, j0=j0, j1=j1lower, tau=CURRENT_RAMPTIME,
        time=SIMULATION_TIME, dmi = dmi, infile=infile,
        force_sim=args.force_sim)

    #check if no domain wall was created
    #if a domain wascreated the lower border is to high
    #stop simulation
    print('(II) Performing analysis of simulation data')
    if analysis(alpha=alpha, j0=j0, j1=j1lower, dmi=dmi, tau=CURRENT_RAMPTIME) == True:
        print('No DW Creation in the chosen interval')
        return

#main loop for nested interval method

```

```

#choose NUMBER_OF_LOOPS for required the resolution
for loop in range(NUMBER_OF_LOOPS):

    #simulation for the middle of the electric current interval
    print("(II) Running simulation for alpha={0} ramping from " \
          "j0={1} to j1={2} ...".format(alpha, j0, j1mid))
    current_state = run_simulation(
        alpha=alpha, j0=j0, j1=j1mid, tau=CURRENT_RAMPTIME,
        time=SIMULATION_TIME, dmi = dmi, infile=infile,
        force_sim=args.force_sim)

    # Perform the analysis.
    print('(II) Performing analysis of simulation data to')

    #check if there was domain wall creation with j_mid
    #decide in which half of the interval the critical current value is located
    if analysis(alpha=alpha, j0=j0, j1=j1mid, tau=CURRENT_RAMPTIME, dmi=dmi) == True:
        tmp = j1mid
        j1mid = (j1lower+j1mid)/2
        j1higher = tmp
    else:
        tmp = j1mid
        j1mid = (j1higher+j1mid)/2
        j1lower = tmp

    #save results in a file
    else:
        with open("nanowire_shedding_len={0}_tau={1}_alpha={2}_BDMI={3}".format(
            XNODES, CURRENT_RAMPTIME, alpha, BDMI) + '_interval.txt', 'w') as outfile:
            outfile.write("{0:.8g}\t{1:.8g}\t{2:.8g}\t{3:.8g}\t{4:.8g}".format(
                alpha, dmi, j1lower, j1mid, j1higher))

```

B. Literature

- [1] G. Tatara and H. Kohno, *Physical Review Letters* **92**, 086601 (2004).
- [2] S. Zhang and Z. Li, *Physical Review Letters* **93**, 127204 (2004).
- [3] A. Thiaville, Y. Nakatani, J. Miltat, and Y. Suzuki, *Europhysics Letters* **69**, 990 (2005).
- [4] A. Brataas, A. D. Kent, and H. Ohno, *Nature Materials* **11**, 372 (2012).
- [5] O. A. Tretiakov, D. Clarke, G. W. Chern, Y. B. Bazaliy, and O. Tchernyshyov, *Physical Review Letters* **100**, 127204 (2008).
- [6] O. A. Tretiakov, Y. Liu, and A. Abanov, *Physical Review Letters* **108**, 247201 (2012).
- [7] D. R. Rodrigues, K. Everschor-Sitte, O. A. Tretiakov, J. Sinova, and A. Abanov, *Physical Review B* **95**, 174408 (2017).
- [8] S. S. P. Parkin, M. Hayashi, and L. Thomas, *Science* **320**, 190 (2008).
- [9] X. Jiang, L. Thomas, R. Moriya, M. Hayashi, B. Bergman, C. Rettner, and S. S. Parkin, *Nature Communications* **1**, 25 (2010).
- [10] R. Tomasello, E. Martinez, R. Zivieri, L. Torres, M. Carpentieri, and G. Finocchio, *Scientific Reports* **4**, 6784 (2014).
- [11] M. Sitte, K. Everschor-Sitte, T. Valet, D. R. Rodrigues, J. Sinova, and A. Abanov, *Physical Review B* **94**, 064422 (2016).
- [12] K. Everschor-Sitte, M. Sitte, T. Valet, A. Abanov, and J. Sinova, *New Journal of Physics* **19**, 092001 (2017).
- [13] M. Stier, W. Häusler, T. Posske, G. Gurski, and M. Thorwart, *Physical Review Letters* **118**, 267203 (2017).
- [14] F. Büttner, I. Limesh, M. Schneider, B. Pfau, C. M. Günther, P. Helsing, J. Geilhufe, L. Caretta, D. Engel, B. Krüger, J. Viehhaus, S. Eisebitt, and G. S. Beach, *Nature Nanotechnology* **12**, 1040 (2017).
- [15] A. Kosevich, B. Ivanov, and A. Kovalev, *Physics Reports* **194**, 117 (1990).
- [16] A. Hubert and R. Schäfer, *Magnetic Domains: The Analysis of Magnetic Microstructures* (Springer-Verlag Berlin Heidelberg, Germany, 1998).

B. Literature

- [17] N. L. Schryer and L. R. Walker, *Journal of Applied Physics* **45**, 5406 (1974).
- [18] R. Gross and A. Marx, *Festkörperphysik* (Oldenbourg Wissenschaftsverlag GmbH, Germany, 2012).
- [19] I. Dzyaloshinskii, *Journal of Physics and Chemistry of Solids* **4**, 241 (1958).
- [20] T. Moriya, *Phys. Rev. Lett.* **4**, 228 (1960).
- [21] I. E. Dzyaloshinskii, *Jetp* **19**, 960 (1964).
- [22] O. A. Tretiakov and A. Abanov, *Physical Review Letters* **105**, 157201 (2010).
- [23] A. A. Thiele, *Physical Review Letters* **30**, 230 (1973).
- [24] D. R. Rodrigues, A. Abanov, J. Sinova, and K. Everschor-Sitte, *Physical Review B* **97**, 134414 (2018).
- [25] T. L. Gilbert, *IEEE Transactions on Magnetics* **40**, 3443 (2004).
- [26] L. D. Landau and E. M. Lifshitz, *Phys. Z. Sowjetunion* **8**, 153 (1935).
- [27] M. Dyakonov and V. Perel, *Physics Letters A* **35**, 459 (1971).
- [28] J. E. Hirsch, *Physical Review Letters* **83**, 1834 (1999).
- [29] J. Sinova, S. O. Valenzuela, J. Wunderlich, C. H. Back, and T. Jungwirth, *Reviews of Modern Physics* **87**, 1213 (2015).
- [30] J. Sinova, D. Culcer, Q. Niu, N. A. Sinitsyn, T. Jungwirth, and A. H. MacDonald, *Physical Review Letters* **92**, 126603 (2004).
- [31] R. Ramaswamy, J. M. Lee, K. Cai, and H. Yang, *Applied Physics Reviews* **5**, 031107 (2018).
- [32] J. Slonczewski, *Journal of Magnetism and Magnetic Materials* **159**, L1 (1996).
- [33] L. Berger, *Physical Review B* **54**, 9353 (1996).
- [34] S. Zhang, P. M. Levy, and A. Fert, *Physical Review Letters* **88**, 2366011 (2002).
- [35] M. Hayashi, J. Kim, M. Yamanouchi, and H. Ohno, *Physical Review B* **89**, 144425 (2014).
- [36] D. C. Ralph and M. D. Stiles, *Journal of Magnetism and Magnetic Materials* **321**, 2508 (2009).
- [37] A. Chernyshov, M. Overby, X. Liu, J. K. Furdyna, Y. Lyanda-Geller, and L. P. Rokhinson, *Nature Physics* **5**, 656 (2009).
- [38] I. Mihai Miron, G. Gaudin, S. Auffret, B. Rodmacq, A. Schuhl, S. Pizzini, J. Vogel, and P. Gambardella, *Nature Materials* **9**, 230 (2010).

B. Literature

- [39] L. Liu, T. Moriyama, D. C. Ralph, and R. A. Buhrman, Physical Review Letters **106**, 036601 (2011).
- [40] L. Liu, C. F. Pai, Y. Li, H. W. Tseng, D. C. Ralph, and R. A. Buhrman, Science **336**, 555 (2012).
- [41] S. Rohart and A. Thiaville, Physical Review B **88**, 184422 (2013).
- [42] N. Sommer, “ Bachelorthesis: Stromgetriebene Domänenwanderzeugung in ferromagnetischen Nanodrähten ,” (2017).
- [43] J. Shibata, G. Tatara, and H. Kohno, Physical Review Letters **94**, 076601 (2005).
- [44] *MicroMagnum is a fast micromagnetic simulator for computations on CPU and GPU , micromagnum.informatik.uni-hamburg.de.*
- [45] K. M. Hals and K. Everschor-Sitte, Physical Review Letters **119**, 127203 (2017).
- [46] K. Litzius, “Spin-Orbit-Induced Dynamics of Chiral Magnetic Structures,” (2018).

C. Acknowledgment

I would like to thank my supervisor Dr. Karin Everschor-Sitte for providing me this interesting topic and for the support during the year of my Master research. Another special thank goes to Dr. Davi Rohe Rodrigues for his support and assistance when I was at a problem point. Both have always taken time to answer my questions or having inspiring discussions on my topic. Further I like to thank for their hints and improvements for my scientific writing.

I thank Benjamin McKeever, Venkata Krishna Bharadwaj and Dr. Kai Litzius for their support whenever there were problems with MicroMagnum and their explanations about the functionality of this simulation tool. I thank my office colleague Timo Pulch for his suggestions and the discussions about my topic, and I like to extend my thanks to the entire TWIST Group for the support and for providing a computer to run my simulations.

I thank Prof. Dr. Friederike Schmid as the second reviewer of this thesis, and last but not least I would like to thank my friends and family for their continuous support.